JPL Publication 87-43

Space Science/Space Station Attached Payload Pointing Accommodation Study

Technology Assessment White Paper

Richard Y. Lin
Kenneth E. Mann
Robert A. Laskin
Samuel W. Sirlin

December 15, 1987

National Aeronautics and Space Administration

Jet Propulsion Laboratory
California Institute of Technology
Pasadena, California

TECHNICAL REPORT STANDARD TITLE PAGE

1. Report No. 87-43	2. Government Accession No.	3. Recipient's Catalog No.
4. Title and Subtitle Space Science/Space Station Attached Payload Pointing Accommodation Study Technology Assessment White Paper		5. Report Date December 15, 1987 6. Performing Organization Code
7. Author(s) Richard Y. Lin, Kenneth E. Mann, Robert A. Laskin, Samuel W. Sirlin		8. Performing Organization Report No.
9. Performing Organization Name and Address JET PROPULSION LABORATORY California Institute of Technology 4800 Oak Grove Drive Pasadena, California 91109		10. Work Unit No. 11. Contract or Grant No. NAS7-918 13. Type of Report and Period Covered External Report JPL Publication
12. Sponsoring Agency Name and Address NATIONAL AERONAUTICS AND SPACE ADMINISTRATION Washington, D.C. 20546		14. Sponsoring Agency Code RE4 BP-186-02-04-02-00

15. Supplementary Notes

16. Abstract

Technology assessment is performed for pointing systems that accommodate payloads of large mass and large dimensions. Related technology areas are also surveyed. These related areas include active thermal lines or power cables across gimbals, new materials for increased passive damping, tethered pointing, and inertially reacting pointing systems. Conclusions, issues and concerns, and recommendations regarding the status and the development of large pointing systems for space applications are made based on the performed assessments.

17. Key Words (Selected by Author(s))	18. Distribution Statement		
Launch Vehicles and Space Vehicles; Spacecraft Design, Testing, and Performance	Unclassified; unlimited		
19. Security Classif. (of this report)	20. Security Classif. (of this page)	21. No. of Pages	22. Price
Unclassified	Unclassified		

HOW TO FILL OUT THE TECHNICAL REPORT STANDARD TITLE PAGE

Make items 1, 4, 5, 9, 12, and 13 agree with the corresponding information on the report cover. Use all capital letters for title (item 4). Leave items 2, 6, and 14 blank. Complete the remaining items as follows:

3. Recipient's Catalog No. Reserved for use by report recipients.

7. Author(s). Include corresponding information from the report cover. In addition, list the affiliation of an author if it differs from that of the performing organization.

8. Performing Organization Report No. Insert if performing organization wishes to assign this number.

10. Work Unit No. Use the agency-wide code (for example, 923-50-10-06-72), which uniquely identifies the work unit under which the work was authorized. Non-NASA performing organizations will leave this blank.

11. Insert the number of the contract or grant under which the report was prepared.

15. Supplementary Notes. Enter information not included elsewhere but useful, such as: Prepared in cooperation with... Translation of (or by)... Presented at conference of... To be published in...

16. Abstract. Include a brief (not to exceed 200 words) factual summary of the most significant information contained in the report. If possible, the abstract of a classified report should be unclassified. If the report contains a significant bibliography or literature survey, mention it here.

17. Key Words. Insert terms or short phrases selected by the author that identify the principal subjects covered in the report, and that are sufficiently specific and precise to be used for cataloging.

18. Distribution Statement. Enter one of the authorized statements used to denote releasability to the public or a limitation on dissemination for reasons other than security of defense information. Authorized statements are "Unclassified–Unlimited," "U. S. Government and Contractors only," "U. S. Government Agencies only," and "NASA and NASA Contractors only."

19. Security Classification (of report). NOTE: Reports carrying a security classification will require additional markings giving security and downgrading information as specified by the Security Requirements Checklist and the DoD Industrial Security Manual (DoD 5220.22-M).

20. Security Classification (of this page). NOTE: Because this page may be used in preparing announcements, bibliographies, and data banks, it should be unclassified if possible. If a classification is required, indicate separately the classification of the title and the abstract by following these items with either "(U)" for unclassified, or "(C)" or "(S)" as applicable for classified items.

21. No. of Pages. Insert the number of pages.

22. Price. Insert the price set by the Clearinghouse for Federal Scientific and Technical Information or the Government Printing Office, if known.

JPL Publication 87-43

Space Science/Space Station Attached Payload Pointing Accommodation Study

Technology Assessment White Paper

Richard Y. Lin
Kenneth E. Mann
Robert A. Laskin
Samuel W. Sirlin

December 15, 1987

National Aeronautics and
Space Administration

Jet Propulsion Laboratory
California Institute of Technology
Pasadena, California

The research described in this publication was carried out by the Jet Propulsion Laboratory, California Institute of Technology, under a contract with the National Aeronautics and Space Adminstration.

ABSTRACT

Technology assessment is performed for pointing systems that accommodate payloads of large mass and large dimensions. Related technology areas are also surveyed. These related areas include active thermal lines or power cables across gimbals, new materials for increased passive damping, tethered pointing, and inertially reacting pointing systems. Conclusions, issues and concerns, and recommendations regarding the status and the development of large pointing systems for space applications are made based on the performed assessments.

CONTENTS

1.0 OBJECTIVES

Technology assessment is one of the work elements in the Space Science/Space Station attached payload pointing accommodation study. The relations among work elements are illustrated in Figure 1.1. The primary objective of this technology assessment was to determine pointing technology readiness in meeting Space Science (Code E) requirements.

The survey of current pointing capabilities, technology maturity, and projection of technology trends will also generate data needed for pointing system performance analysis and simulation. For example, the technology survey will identify sensor accuracies, actuator torque limits, material damping levels, and control methodologies all of which are needed in pointing performance simulation. Moreover, technology assessment will also survey previous pointing architectures, thereby generating preliminary concepts for the architectural options study.

2.0 SCOPE

The technology assessment reported herein is specifically intended for the Space Science/Space Station attached payload pointing accommodation study. Emphasis was placed on relatively large pointing systems and components, capable of accommodating a payload mass of 600 kg to 6000 kg. Major areas surveyed include: gimbaled pointing systems, isolation systems, sensors, actuators, and control methodologies.

In the course of the technology assessment other technology areas, considered important or relevant to the overall Code E pointing needs, were addressed. These areas include: tethered pointing platforms or payloads, active thermal control lines across gimbals, power/data cables crossing axes of rotation, and new materials for increased passive damping.

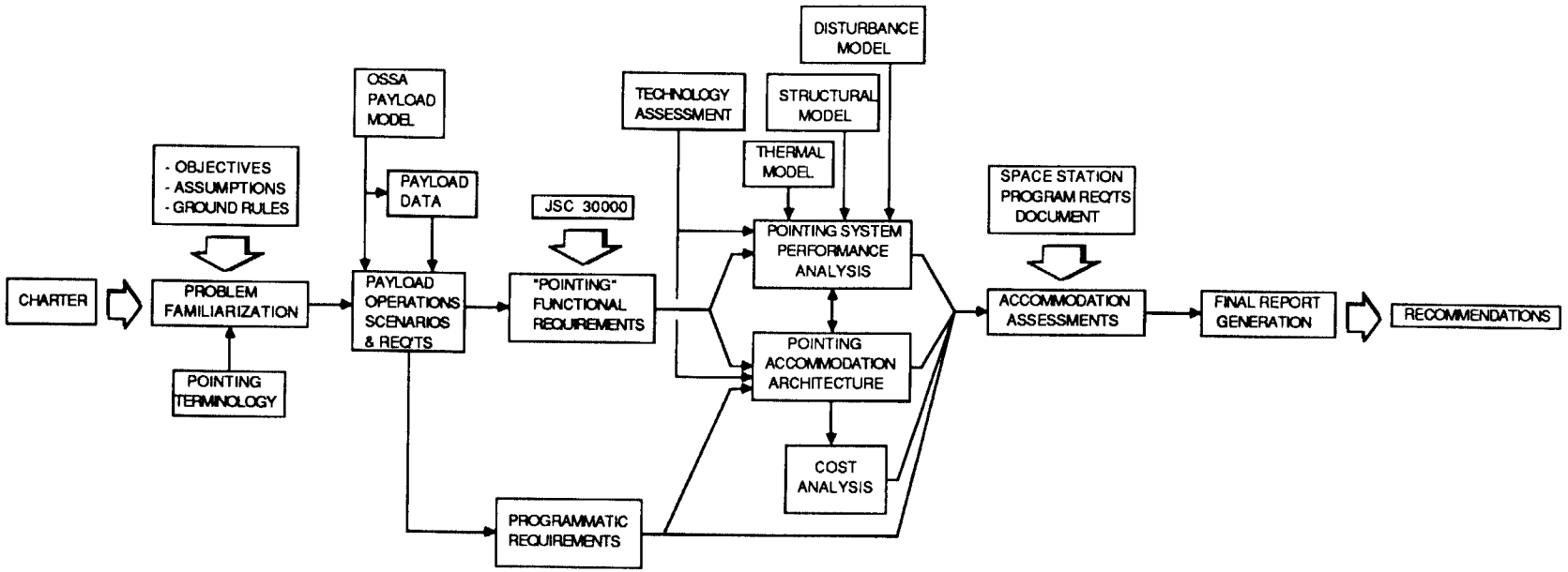

Figure 1.1
Code E Study Flow Chart

3.0 APPROACH

The fundamental approach taken is that of reviewing and updating a previous technology assessment report [1] and of undertaking a new survey of areas that were not included in the previous work.

In 1984, a pointing system technology assessment was performed by the Jet Propulsion Laboratory for space science and Space Station missions in the 1990s. The results were documented in the report entitled "Advanced Precision Pointing System Technology Assessment" and were reported in the open literature [1]. In 1986, a gimbal systems survey was performed, which represented an update of gimbal systems from the 1984 report. These two results were used as the starting data base for this work. A significant effort was then undertaken to update this data base by literature search and by visits to selected organizations and companies to obtain information on developments made in the past three years (1984-1987).

In addition, a new survey was performed for several areas not included in the previous technology assessment. This survey was completed by collecting information from appropriate reports and from discussions with various pointing system analysts and designers around the country.

4.0 TECHNOLOGY ASSESSMENT RESULTS

4.1 Gimbaled Pointing Systems

4.1.1 Introduction

This study considers gimbal systems designed to carry large payloads in space. Only three large gimbal systems have been flown. These are the 3-axis Apollo Telescope Mount (ATM) which flew on Skylab, the 3-axis Instrument Pointing System (IPS) which flew on the Space Shuttle, and the single-axis Cryogenic Infrared Radiance Instruments for Shuttle (CIRRIS-1), which also flew on the Shuttle, STS-4. One large 2-axis gimbal system, CIRRIS-1A, was delivered to USAF/AFGL for Shuttle flight STS-62A in 1986, but the Shuttle flight has been delayed. Another large 2-axis gimbal system, the Two Axis Pointing System (TAPS), is scheduled for delivery to Goddard Space Flight Center in March 1988.

In addition to the gimbal systems that have been fabricated or are under construction, other systems are reviewed. These include pointing systems designed for the Shuttle which have reached various stages of design and fabrication before cancelation. A brief section on ground gimbal systems is included in order to acquaint readers with some of the capabilities of large ground gimbal systems manufactured for flight simulators that may be adaptable to the Space Station needs.

4.1.2 Flown Gimbal Systems

This section reviews the three pointing systems which have flown, ATM, IPS and CIRRIS-1. ATM flew on Skylab, and the last two flew on the Space Shuttle.

The Apollo Telescope Mount (ATM) [2] was designed and developed to house and support manned telescopes for studying the sun. The objective of the ATM was to carry and point solar instruments to acquire high-resolution observations of the structure and behavior of the sun from above the earth's atmosphere. The ATM was a 10,000 kg octagonally shaped structure. The structural frame surrounded a large cylindrical canister housing the scientific instruments. The cylinder measured 2.13 meters in diameter and 3.35 meters in length. The ATM can support up to 1000 kg of experiment instrumentation. The Skylab provided the coarse pointing while the Experiment Pointing Control system provided fine pointing and stabilization. The coarse pointing system CMGs maintained the Skylab position to within 3 arc-minutes of the desired angular position. The center of mass mounted 3-axis gimbal system (pitch, yaw, roll) provided pitch and yaw control to within 2.5 arc-seconds for periods up to 15 minutes by utilizing fine-pointing sun sensors as attitude reference. Operation of the instruments required crew participation to respond to transient solar phenomena. The ATM flew in 1973 on Skylab.

The Instrument Pointing System (IPS) is a gimbal system which is mounted on an open pallet sitting in the open bay of the Space Shuttle. It provides 3 degrees of freedom (pallet to payload: azimuth, cross elevation, elevation) to an end mounted payload. All experiments are fully exposed to space. The IPS subassemblies are gimbal structure, drive, thermal control, payload clamp, attitude measurement, power electronics, and data electronics. Total IPS mass is 750 kg. The IPS has a pointing accuracy of 30 microradians, stability of approximately 18 microradians, maximum slew rate of 56 millirad/sec, and maximum torque of 23 newton-meters per axis. The IPS provides for payload masses in the range of 200 to 2500 kg and moments of inertia up to approximately 2000 kg-m^2.

Cryogenic Infrared Radiance Instruments for Shuttle, CIRRIS-1, [3,4], is a single axis pointing system for an infrared telescope system developed for the Air Force Geophysics Laboratory. It is a pallet-fixed aluminum H-beam structure weighing 350 kg with excursion in pitch limited to -15° to 0°. It was designed to point a payload of 600 kg with a size of 0.965 meter diameter by 2.97 meter length to an accuracy of 12 arc-minutes. With the Shuttle in a nose-down attitude, CIRRIS-1 used the Shuttle orbital motion to provide a translational scan along the limb and a single axis pointing control to step through a sequence of tangent heights. That is, the instrument is programmed to perform a series of horizontal scans, stepped in elevation, with step duration on the order of 10 seconds. The transition time between elevation steps is approximately 1 second, and the step size is on the order of 1 degree. The total scan duration for a complete atmospheric sample was approximately 100 seconds. CIRRIS-1 consists of an elevation sensor mount driven by high precision direct drive (gearless) torquer motors which are controlled by a microprocessor based servo control system. Figures of merit for the full system include a 1 arc-minute absolute pointing accuracy, a line of sight drift error of 10 arc-seconds/sec for any 10 second duration and a jitter stability of 5 arc-seconds. Although the torquer motor had a rated maximum torque of 135 N-m, the output was limited to 60 N-m by an imposed 100 watt power limitation.

4.1.3 Delivered Gimbal System (CIRRIS-1A)

Cryogenic Infrared Radiance Instruments for Shuttle (CIRRIS-1A) is a two-axis azimuth-over-elevation direct-drive mount developed for the Air Force Geophysics Laboratory to carry instruments to measure emissions in the 2.5 to 25 micron region. CIRRIS-1A has a payload capacity of 680 kg with dimensions of 0.965 meter diameter by 2.82 m length with a pointing accuracy of 4 arc-minutes. Its gimbal structure is box beam with a weight of 940 kg. The excursion limits are pitch: -24.5° to 6°; roll: $\pm$38°. Torquer motors are used in both axes without gear trains to produce a smooth and accurate positioning.

CIRRIS-1A was delivered for scheduled Space Shuttle flight SST-62A. Due to the Challenger accident, its flight has been delayed.

4.1.4 Gimbal System Under Fabrication (TAPS)

The Two-Axis Pointing System (TAPS) is a center of mass (c.m.) mount two-axis gimbal system designed for Goddard Space Flight Center. This system is intended to provide arc-minute accuracy pointing for Shuttle payloads weighing up to 1135 kg and sizes up to 1 m x 1 m x 4.2 m length with excursion limits of $\pm 20°$ in pitch and roll. The payload moments of inertia can be as large as 620 N-m^2 for each of the transverse axes and 50 N-m^2 for the longitudinal axis. The TAPS gimbal has a square inner and outer box beam structure and a mass of 1360 kg. The inner dimension is a 1 meter square, and the outer dimension is a 2.8 meter square. Delivery is expected to be made in June 1988, and the first flight has been tentatively scheduled for November 1989. Two identical gimbal systems are under construction.

4.1.5 Brassboard Gimbal Systems

A number of large gimbal systems have been designed for space applications. These systems have reached various stages of completion in demonstrating their concepts and capabilities. Table 4.1.5.1, [1], summarizes these systems in terms of their design goals and capabilities. The acronyms used in the table have the following definitions:

TAGGS - Talon Gold Gimbal System (Lockheed)
LMSC/CG - Lockheed center of gravity mounted gimbal system
GOS - Gimbal Orientation System (Lockheed)
AGS - Advanced Gimbal System (Sperry)
ASPS - Annular Suspension and Pointing System (Sperry)
MMC - Martin Marietta Corporation gimbal system
RG - Reactuator Gimbal (JPL)

From examination of Table 4.1.5.1, it is seen that these systems are all intended for payloads of 1000 kg or greater, but that the torque levels are limited to less than 35 newton-meters. Their pointing and stability performances vary from 3 to 30 microradians. The only exception is ASPS, which is a vernier magnetic stage residing on the AGS. It has a goal of achieving 0.05 arc-seconds pointing and stability. This does point out that for a pointing system to achieve a high degree of pointing performance, an isolation and vernier control will have to be incorporated as part of the design of every pointing system which uses the Space Station coarse pointing system.

The stability numbers listed in Table 4.1.5.1 assume a Space Shuttle disturbance environment which is quieter than the Space Station environment. The stabilities can be expected to be poorer than the values listed in the table if the gimbal system is used on the Space Station. The Reactuator gimbal system is the only one listed in the table to implement reactionless actuators. In this system the actuation does not torque against the basebody on which the gimbal is mounted. More discussion on reactionless actuation is presented in section 4.3.5.

Table 4.1.5.1
Brassboard Gimbal Systems

	TAGGS	LMSC/CG	GOS	ASPS	AGS	MMC	RG
POINTING (μrad)	9	30	150	0.05	40	29	1500
STABILITY (μrad,s)	3,NS	5,NS	25,NS	0.05,NS	12,NS	15,NS	15, 0.033
SLEW RATE (mrad/s)	16	>48	>48	52	70	>48	70
ACCELERATION (mrad/s^2)	2.1	21	>21	10	14	>2.5	1.5
TORQUE (N-m)				34	34		
FOV (deg)	135	180	160	200/120	140	140	$\pm$50/axis
SERVO BW (Hz)	0.5	>0.5	>0.5	1.0	1.0	0.5	0.5
PAYLOAD MASS (kg)	2000	2400	2400	60-7200	0-7200	2000	1000
PAYLOAD INERTIA (kg-m^2)	3500	3500	3500			3500	700

NS = not specified

4.1.6 State-of-the-Art-Gimbal Systems Survey

Large gimbal systems that are ready to support flight missions are listed in Table 4.1.6.1. It is seen that three have been used in flight, one is delivered and one is undergoing fabrication and test. These systems represent the current state of gimbal technology.

Table 4.1.6.1 shows that no payload greater than 2500 kg can be accommodated by current gimbal systems. It also shows that no existing gimbal system can deliver a 15 arc-second stability as required by Code E missions, except IPS and ATM. However, ATM can achieve better than 15 arc-second stability because it is a vernier stage of Skylab. For this reason, it should not be considered as a coarse pointer. IPS achieves 2 arc-second stability under the quiescent Shuttle environment. However, its stability degrades to about 15 arc-seconds due to Shuttle vernier thruster firings alone. IPS cannot be expected to meet Code E stability requirements of 15 arc-seconds when it is operated on the Space Station where disturbances are much more severe than on the Space Shuttle.

4.1.7 Ground Systems

In addition to aerospace companies, there are a number of other companies that fabricate gimbal systems, though only for ground based operation. Many of these gimbal systems are very large. Examples include gimbal systems for very large tracking antennas, flight motion simulators, and guidance and navigational test equipment. None of these gimbals are flight qualified.

One company with experience fabricating large multi-axis flight motion simulators is CARCO Electronics. CARCO Electronics has built a wide variety of gimbal systems for flight simulators. Most of these systems are one of a kind systems and many are very large. As an example, the inside diameter of the second axis on model S-540R-5T is 2.5 m. Typical simulators have 2, 3 or 5 degrees of freedom. While most of the simulators are hydraulically actuated, some models have been built that are actuated by dc torque motors. Table 4.1.7.1 provides data, extracted from the CARCO catalogue, on a few of its gimbal systems. Examples of 2-axis, 3-axis, and 5-axis yokes are listed in the table.

CARCO gimbals are manufactured out of magnesium. Typical cost of a large simulator is on the order of $1 million. The gimbals described in the CARCO catalogue [5] were not designed to accommodate a typical payload mass of the coarse pointing system and thus do not have the necessary stiffness required of the Code E coarse pointing gimbal system.

Table 4.1.6.1
Summary of Flight Gimbal Systems

PROGRAM NAME	MANUFAC-TURER	SPONSOR AGENCY	NO. DEV'D	GIMBAL TYPE	PAYLOAD CAPACITY (kg)	STABILITY (μrad)	STATUS
ATM	Perkin-Elmer	NASA		3-AXIS	1000	15(VERNIER STAGE)	FLOWN
IPS	Dornier	NASA		3-AXIS;STACKED END MOUNTED	2500	10 QUIESCENT	FLOWN
CIRRIS-1	SDC	USAF/AFGL	1	SINGLE AXIS	590	24*	FLOWN
CIRRIS-1A	SDC	USAF/AFGL	1	DUAL-AXIS NESTED FRAME	680	24^{+}	DELIVERED FOR FLT 86
TAPS	SDC	NASA/GSFC	2	DUAL-AXIS NESTED FRAME	1130	150**	SCHEDULED DEL MAR 88

* Stability requirement; stability in flight is not available
\+ Stability requirement
** Stability specification for flight system; however, the manufacturer expects a stability of 21 μ rad.

Table 4.1.7.1
Summary of Some CARCO Gimbal Systems [5]

MODEL NUMBER	DESCRIPTION	LOAD SIZE	RESOLUTION (deg)
S-450	3-AXIS	24"DIA X 21" LONG	0.02
S-460	3-AXIS ELECTRIC	24"DIA X 24" LONG	0.0001 (.36 arc-sec)
S-458R-3	3-AXIS OPEN GIMBAL	16"DIA X 60" LONG	0.001
S-520-R	3-AXIS YOKE	32"DIAMETER X 80" LENGTH	.05/.035/.035
S-520	2-AXIS YOKE	36" X 35"	NOT LISTED
S-540R-5T	5-AXIS (2-AXIS TARGET, 3-AXIS SIMULATOR)	INNER DIMENSION OF TARGET SIMULATOR EQUALS 101"	.1/.05/.05 .1/.05/.05
S460 R/D	3-AXIS PRECISION	26"DIA X 28" LONG	.1 arc-sec

4.1.8 Conclusions

There does not exist a coarse pointing system which meets the Space Station Code E pointing requirements for space science. Of the five gimbal systems described above (ATM, IPS, CIRRIS-1, CIRRIS-1A, TAPS), the first was designed as a vernier stage for Skylab, and the last four were designed for the Space Shuttle environment. These last four do not meet Space Station requirements in either their ability to accommodate a large payload or to cope with the Space Station disturbances. Only IPS is large enough to accommodate the projected space science payloads. However it is a cantilever pointing system which cannot provide adequate pointing stability in the vibrationally noisy environment of the Space Station. While some of the ground gimbal systems are large enough, they are not sufficiently stiff to meet Space Station requirements. However it may be possible to scale up some of the smaller ground gimbal systems, such as the CARCO model S-520.

4.2 Isolation Systems

4.2.1 Brassboard Development of Isolation Systems

4.2.1.1 Magnetic Suspension

Magnetic suspension is being developed for precision pointing applications in space. It can be used for isolation, pointing or positioning. Some of the programs that it has been applied to are the Annular Suspension Pointing System (ASPS), Space Active Vibration Isolator (SAVI), Figure 4.2.1.1.1 [6], Feamis Active Isolator (6 DOF), and the Talon Gold Magnetic Suspension System (3 DOF). It is also included in the baseline design of SDIO projects employing large precision pointed mirrors. While Feamis is too small for the Space Station coarse pointing system, one of the SDI sponsored systems may be adaptable.

The magnetic actuator has several desirable characteristics. It is possible to apply force in one direction without constraining motion in the other directions. Thus the system is essentially decoupled in each axis. This characteristic permits the control designer to tailor the control law to the payload for each of the degrees of freedom. In addition, while changes in payload or the expected disturbance environment usually require major design changes in mechanical isolators, a magnetic isolation system requires only control law gain changes. As a result, a magnetic isolator can be designed to accommodate a wide range of payload masses and inertias. If the control law is implemented in a digital computer, the suspension can be adjusted after launch to correct for changes in the disturbance environment. The system can be tuned to provide improved performance.

The principal application of magnetic suspension seems to be for isolation where isolation is a secondary function to that of inertial pointing. Inertial sensors are used to point the payload. The advantages of magnetic suspension isolators over mechanical isolators are:

1. superior isolation performance;
2. independent isolation responses for each degree of freedom;
3. accommodation of a wide range of masses and disturbances without major redesign;
4. ability to tune the suspension while in flight;
5. no contacting parts.

The disadvantages are an increase in complexity and a requirement for more operating power. In addition they are load limited. They are also limited to the magnetic gap dimensions which are approximately 1 cm.

There are various types of magnetic suspension systems. The difference depends on the type of actuation sensor used. The actuation sensors used are gap sensors, flux sensors (Hall

probes) or force sensors (quartz crystal). Talon Gold utilizes force sensing, and Feamis uses flux sensing. The Sperry magnetic actuator consists of two electromagnets, a soft iron armature and control and drive electronics.

Comparison of magnetic suspension vs. passive mechanical isolation is presented in Figure 4.2.1.1.2, [6]. Similar diagrams are found in reference [7]. From this Figure it can be seen that magnetic suspension provides superior isolation. Sperry has conducted a test program on a single-axis isolator, [7], to verify the high frequency model and to measure the achievable isolation provided by a system of magnetic actuators. The measured isolation response is shown in Figure 4.2.1.1.3, [7]. The fit of the experimental data with the anticipated results is seen to be very good. Detailed discussions of the data are presented in reference [7].

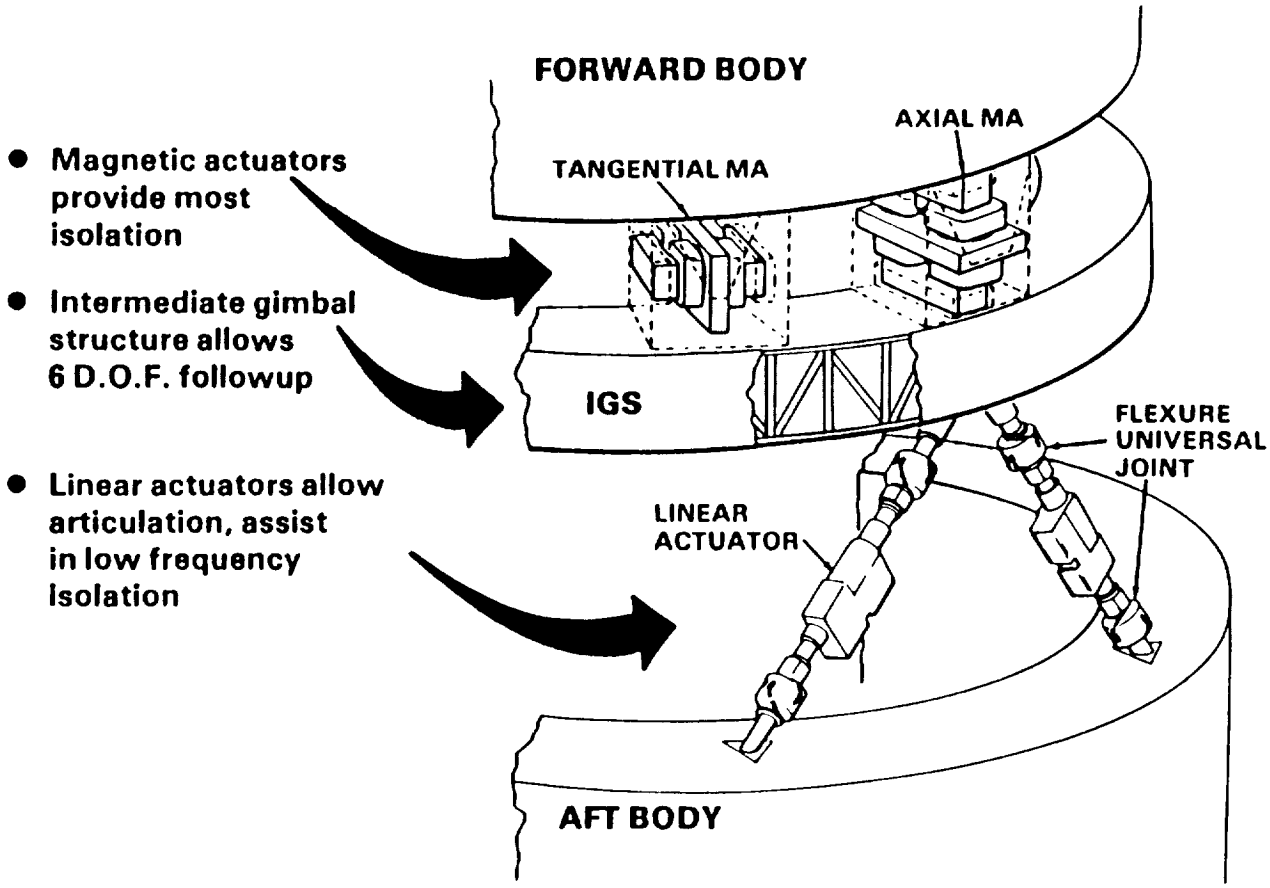

Figure 4.2.1.1.1
SAVI System Configuration [6]

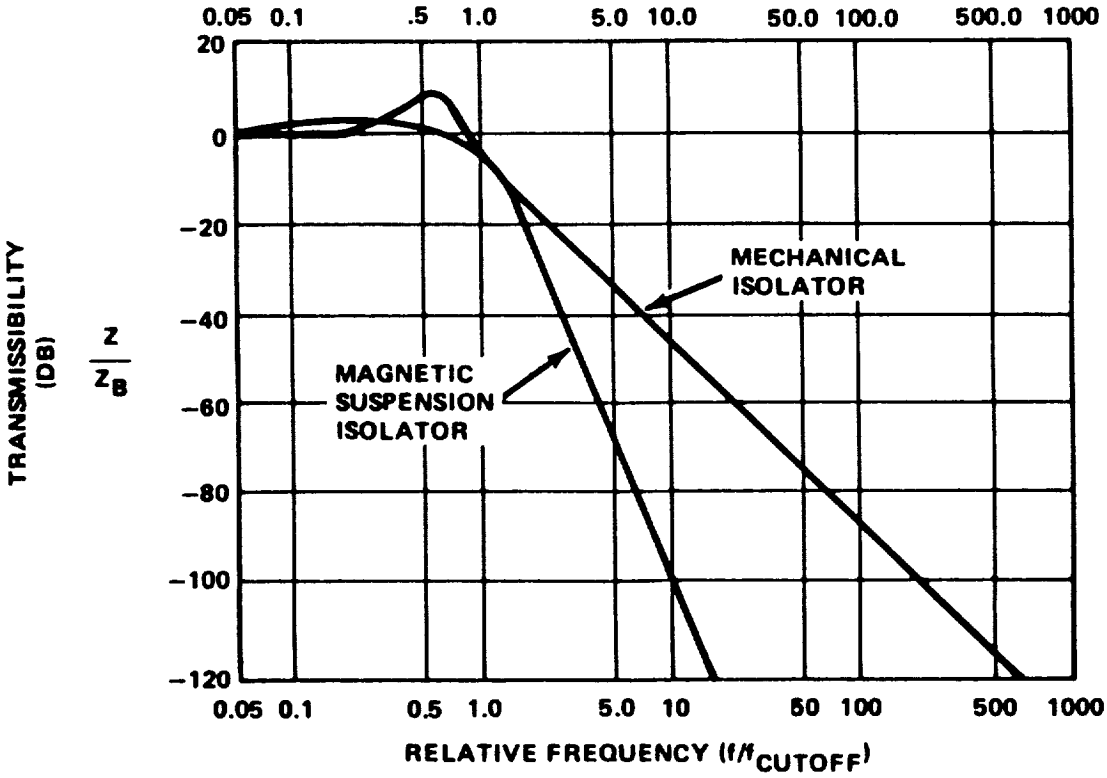

Figure 4.2.1.1.2
Comparison of Magnetic Suspension vs. Passive Mechanical Isolation [6]

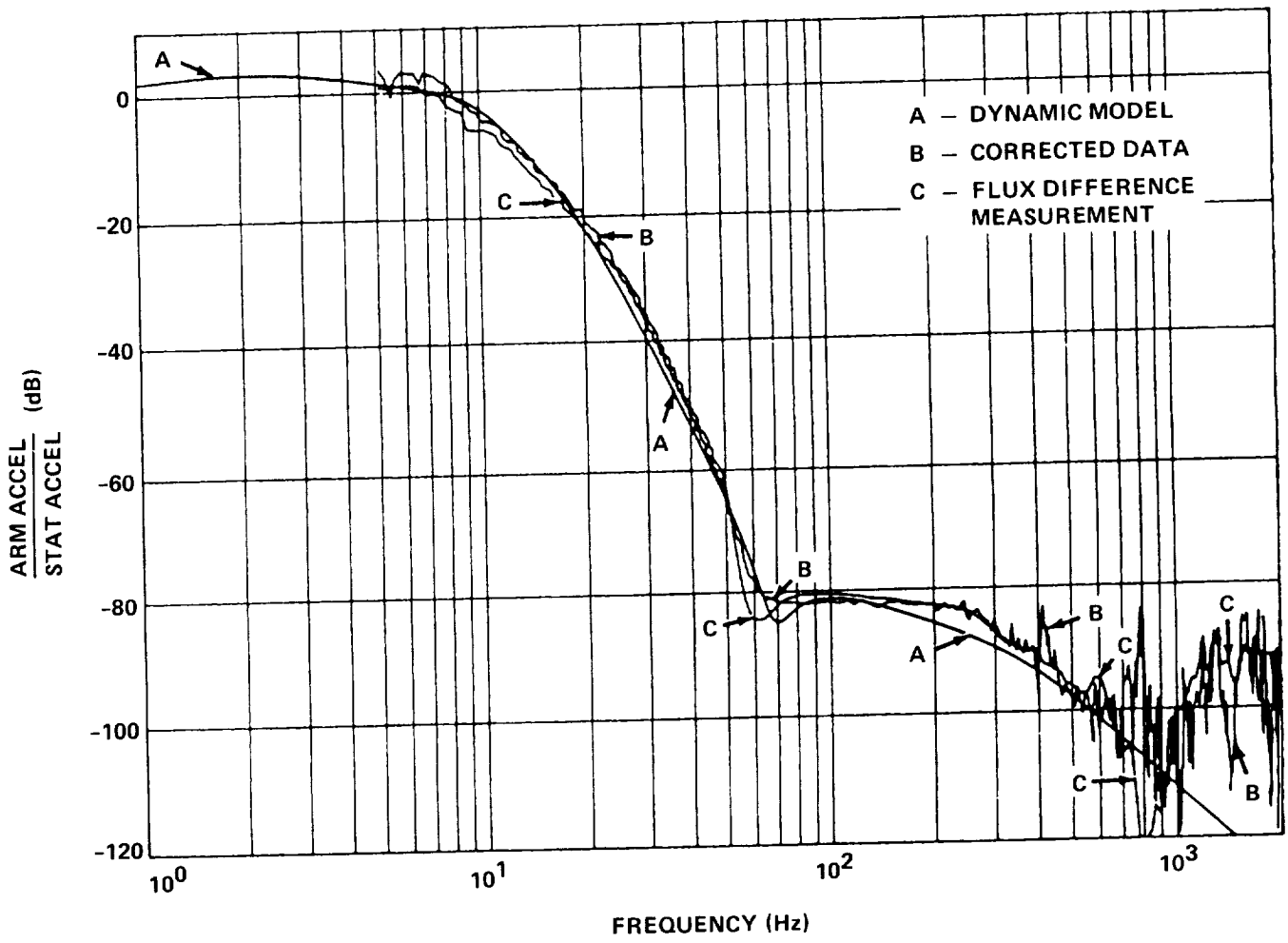

Figure 4.2.1.1.3
Isolation characteristics [7]

4.2.1.2. Gimbalflex

The Gimbalflex system, [8], is a multi-degree of freedom inertial platform intended for payload pointing in a vibration environment. A 5 degree-of-freedom (DOF) Gimbalflex would consist of three linear and two rotational DOF.

The two rotational DOF are implemented with an intermediate gimbal, and the three translational DOF are achieved using an orthogonal linkage system. Its principle is illustrated in Figure 4.2.1.2.1. Plate A in the Figure has a single DOF with respect to plate B along the x-axis. But it is stiff in y and z and all rotational axes. Plate B has a single DOF with respect to plate C along the y-axis. Thus plate A has two DOF with respect to plate C, but remains stiff rotationally. If another linkage set is added orthogonally to the first two, 3 DOF would result.

The relations between the angular and linear freedoms for a typical Gimbalflex system are illustrated in Figure 4.2.1.2.2, in which angular motion is represented by and linear motion is achieved by use of pivots and parallel arms. In this implementation, linear spring constant is a function of the rotation (Bendix) flexure spring constant and length of the parallel arms. The system is designed to have non-intercoupling between angular and linear freedoms. Therefore, a typical angular bandwidth of 30 Hz can be much higher than the linear bandwidth of about 5 Hz.

Gimbalflex has its linkage pivots at the center of percussion, small arm off-null angles, large equivalent payload mass by accelerometer feedback, and spring rate cancellation. These features have contributed to its isolation capability which is at about -70 dB.

There have been 3 DOF (DARPA) and 2 DOF (GAVIS) program demonstrations at Martin Marietta. A multi-pod (6 DOF) concept was under development in 1986. There is on-going development at Martin for the SAVI program of SDIO.

The Gimbalflex suspension system uses mechanical linkages, which are relatively complex. For example, in a three-pod Gimbalflex assembly, each pod consists of 3 translational and 3 rotational linkages, 4 linear actuators and 6 rotational torque motors, 30 flex pivots, 3 accelerometers and 6 capacitor plates, and control electronics.

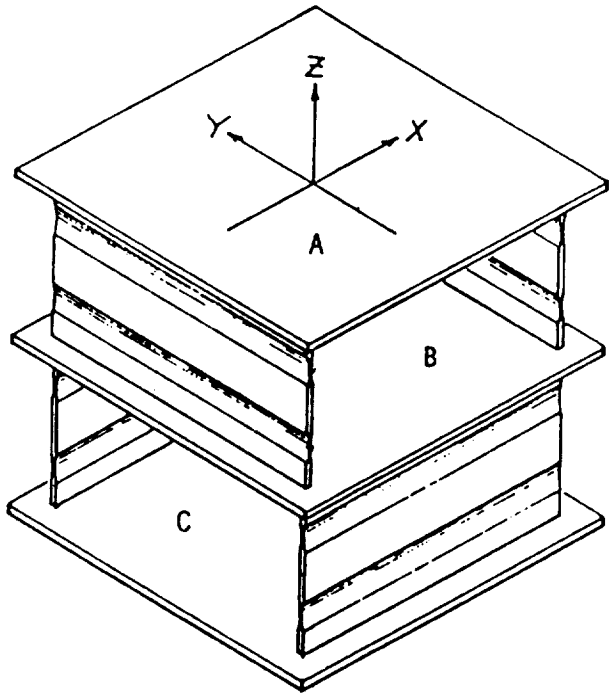

Figure 4.2.1.2.1
Gimbalflex Translation Degrees of Freedom [8]

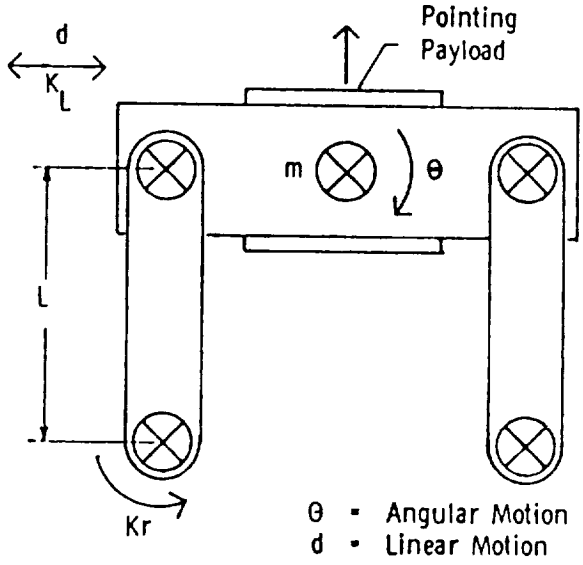

Figure 4.2.1.2.2
Translational and Rotational Degrees of Freedom in Gimbalflex

4.2.2 Isolation System Concepts

4.2.2.1. Suspended Experiment Mount (SEM)

The SEM concept, shown in Figure 4.2.2.1.1, was developed at Marshall Space Flight Center in the early 1980s to provide an experiment mount on the Shuttle for payloads requiring low-g environment, small angle slew and pointing stabilization. The concept consists primarily of a flexible suspension system to passively isolate the payload from high frequency accelerations together with control moment gyros (CMGs) for active control of low frequency disturbances and stabilization of the line of sight.

The suspension system selected for the SEM concept has to be able to isolate the payload from high frequency disturbances while allowing low frequency control of the Shuttle during experiment operation and restrain the payload during periods of high loads such as launch, reentry, and maneuvers. Therefore, the suspension system must be composed of a flexible coupling that can be rigidly locked during periods of high loads. Flexible suspensions considered included elastomeric, wire rope helical spring, solid wire helical spring, and gas filled bellows.

For active control of low frequency disturbances and stabilization of the line of sight, spare Skylab CMGs were considered in SEM. The CMG system is used to control both the payload and, through the suspension system, the Shuttle. The SEM pointing stability was estimated at 1 arc-second.

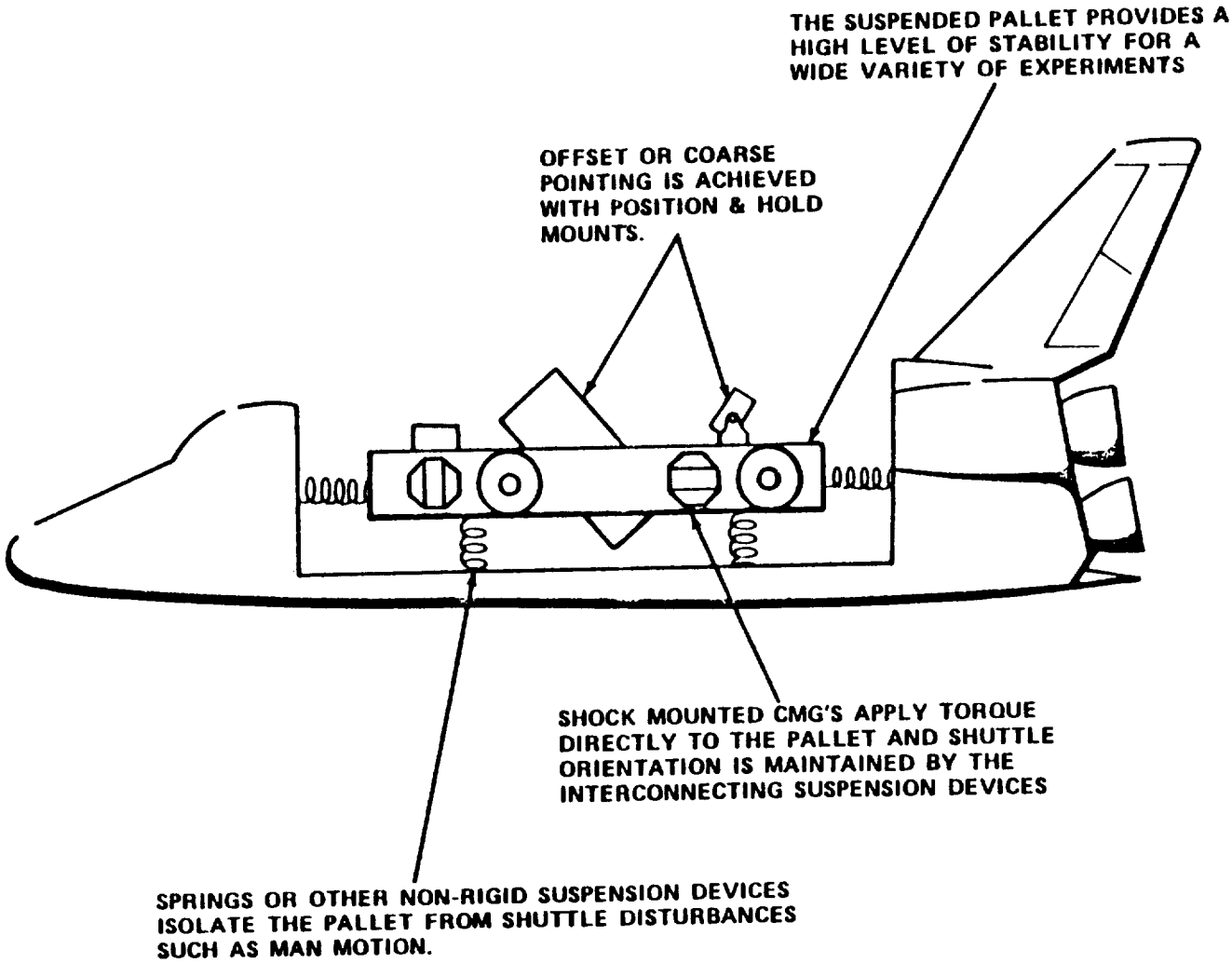

- OTHER FEATURES:
  - NO RCS REQUIRED
  - FULL SKY COVERAGE
  - LOW WEIGHT
  - LARGE MOUNTING SURFACE
  - MINIMUM PALLET/ SHUTTLE INTERFACE

Figure 4.2.2.1.1
Suspended Experimental Mount Concept

4.2.2.2 Six Degree of Freedom Isolator Concept

In 1983, a Shuttle-based flight experiment was proposed to validate large space antenna control technology. To perform a broad spectrum of large antenna flight experiments, a Six Degree of Freedom (6 DOF) isolation concept was developed at the Jet Propulsion Laboratory. A model of the 6 DOF isolator concept is illustrated in Figure 4.2.2.2.1. It has its own sensing and control mechanisms capable of following the payload motion without touching the payload. In this manner, the payload is completely isolated from the basebody (i.e., Shuttle) on which the isolator is mounted.

Depending on the requirements, the isolator tracking volume can be varied using different system designs. For example, for the large antenna experiment, the tracking volume was designed to be 1 cubic meter. When or if the tracking boundary is reached, the isolation system can grab the payload and reposition it to a new starting position.

When this isolation system is used for accommodating pointing payloads, torquers must be mounted on the payloads for inertially reacting actuation. Since the tracking volume may be limited, the duration of complete isolation may be satisfactory only for pointing missions of short periods, unless the payload also has its own translational control, or unless the Shuttle is used in a translational follow up mode.

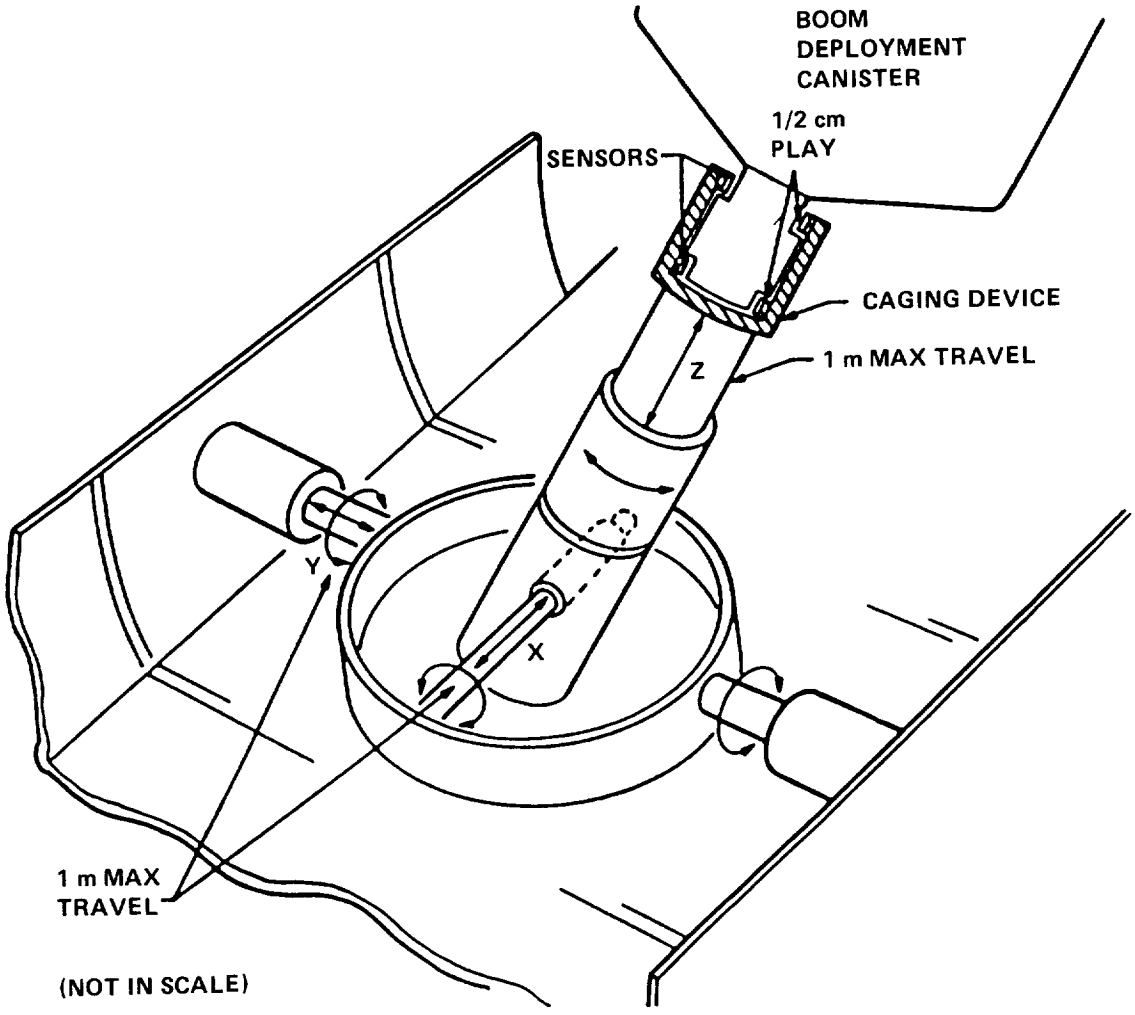

Figure 4.2.2.2.1
Six DOF Isolator Concept

4.2.2.3. Space Telescope Reaction Wheel Isolator

The Hubble Space Telescope isolation system [9] was designed to isolate the telescope from the low level vibration disturbances generated by the attitude control system reaction wheels. The primary goal was to provide isolation from the axial component of wheel disturbance without compromising the control system bandwidth. A passive isolation system was designed employing metal springs in parallel with viscous fluid dampers. The stiffness and damping characteristics have been demonstrated to remain constant over five orders of input disturbance magnitude. The damping remained purely viscous even at the data collection threshold of 0.16 by 10^{-6} to 0.04 inch in input displacement amplitude.

Figure 4.2.2.3.1 [9] presents a diagram of the isolator. Figure 4.2.2.3.2 [9] shows the reaction wheel assembly attached to the isolation system. Figures 4.2.2.3.3 [9] and 4.2.2.3.4 [9] show the radial force measured during a wheel speed rundown without and with isolation. The plots are a composite of force spectra taken at 16 second intervals during a 1600 second reaction wheel assembly (RWA) rundown from 3000 rpm to zero wheel speed. The RWA was back-driven with constant torque so that the wheel speed varied linearly. Harmonic disturbances occur at linearly varying frequencies while resonance in the RWA and test fixtures occurs at constant frequency. Peaking occurs where the two phenomena coincide. The reader should refer to reference [9] for discussion of the data. However, the difference, displayed in the figure, in transmitted energy with and without isolation is dramatic.

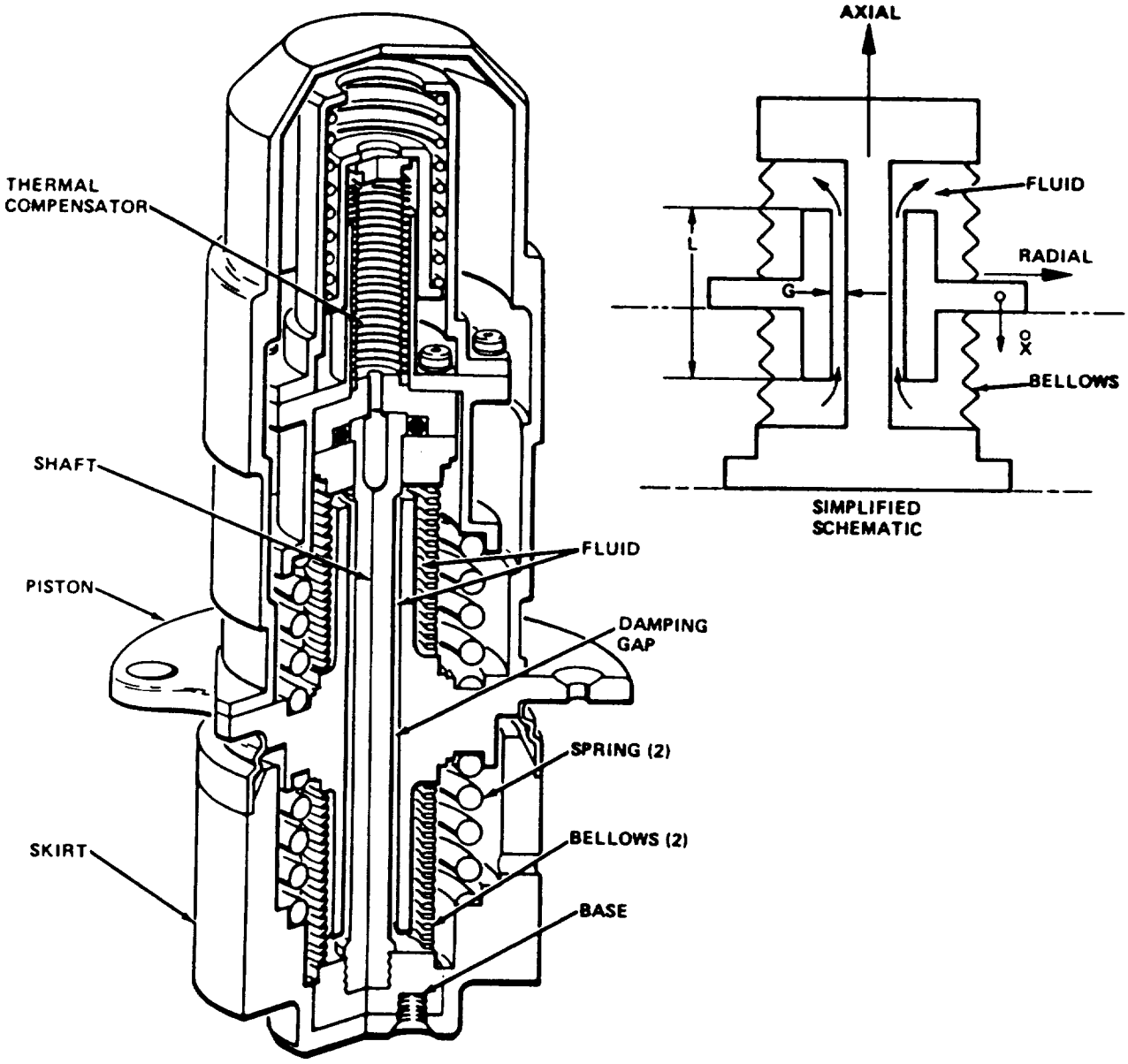

Figure 4.2.2.3.1
Space Telescope Reaction Wheel Isolator Unit [7]

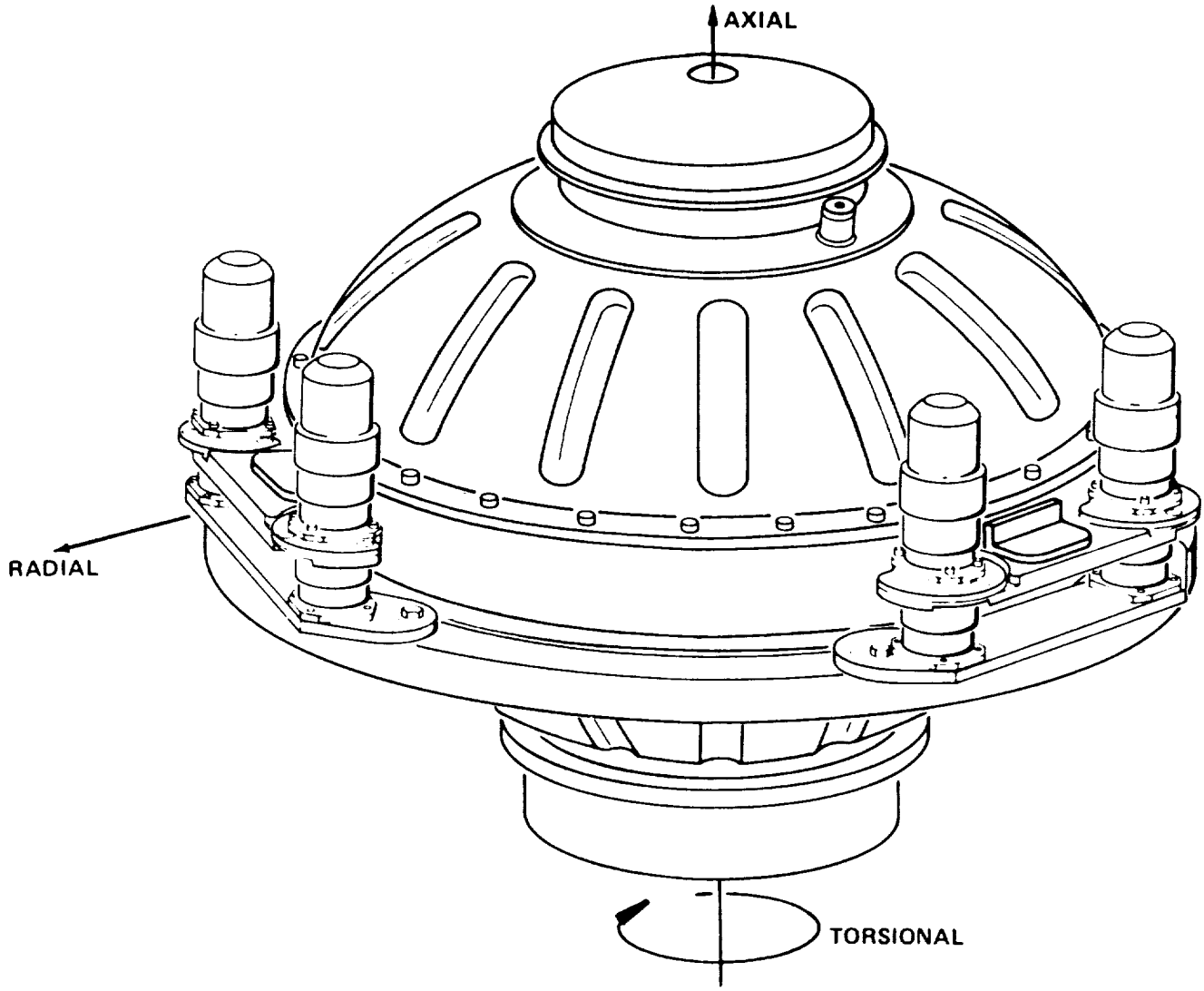

Figure 4.2.2.3.2
Reaction Wheel Assembly Isolation System [9]

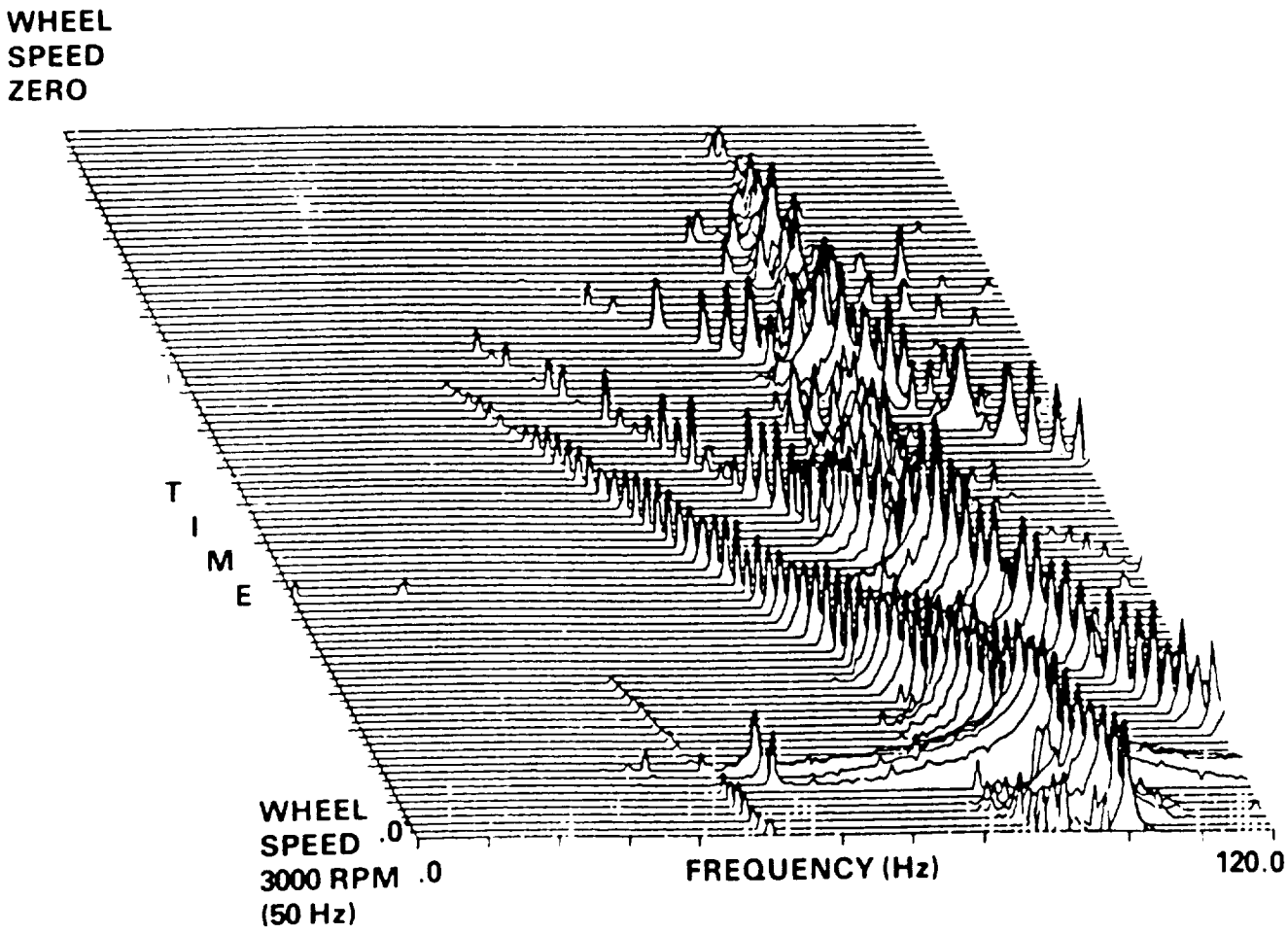

Figure 4.2.2.3.3
Hard Mounted Reaction Wheel Radial Force Plot [9]

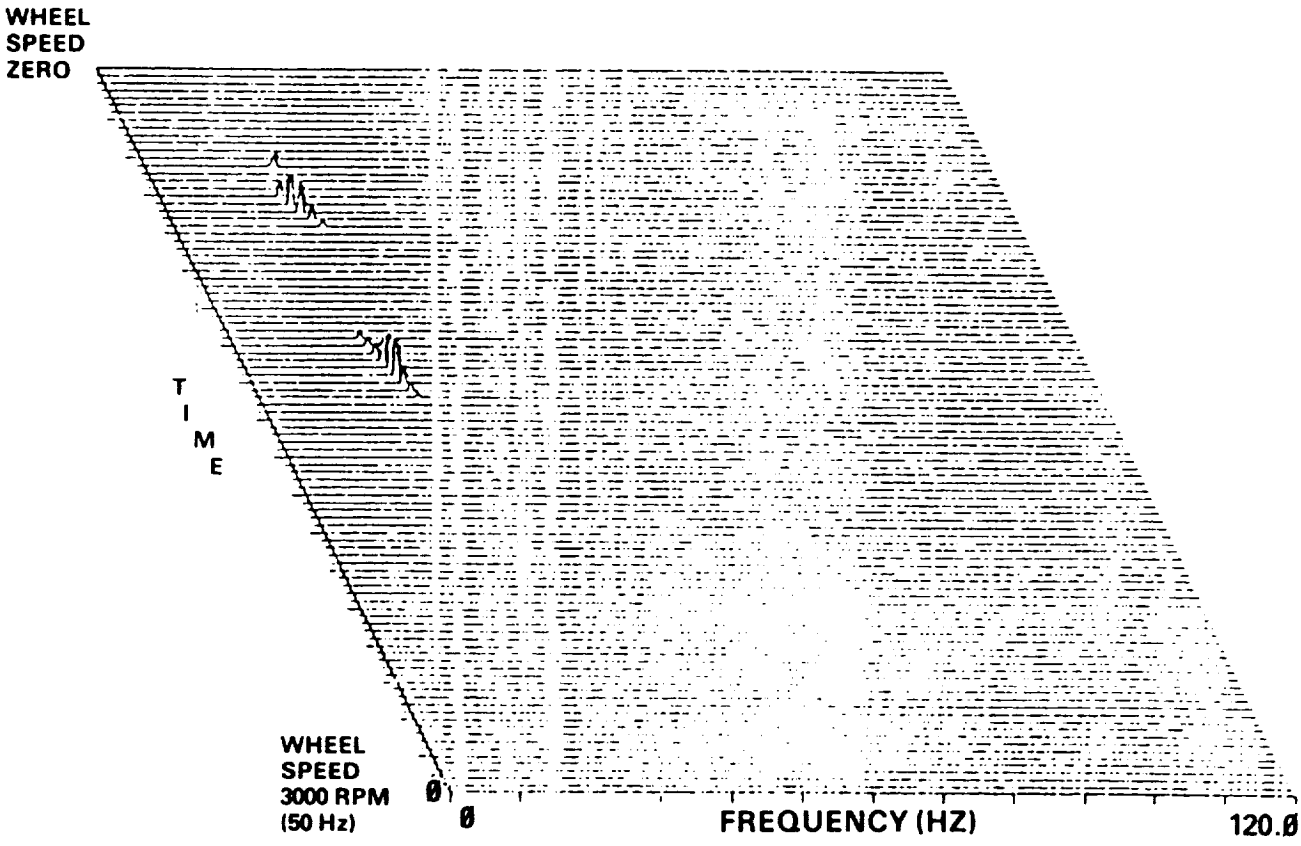

Figure 4.2.2.3.4
Isolated (Sperry Viscous Isolator)
Reaction Wheel Axial Force Plot [9]
(0.052 lb peak) 200 cs fluid

4.3 Sensors and Actuators

4.3.1 Introduction

Table 4.3.1.1 contains a summary of the state-of-the-art in sensor technology for precision pointing, [1,10,11,12,13]. Since the technology assessment of sensors and actuators was made in 1984, [1], and publication of the NASA Space Systems Technology Model, [10], three new devices have been developed. ASTROS (a CCD star tracker) has been delivered, a fiber optic rotation gyro (FORS) brassboard has been fabricated, and an engineering model of a dual motor reactionless actuator has been constructed. Each of these new developments will be discussed below.

Sections 4.3.2, 4.3.3 and 4.3.4 will describe ASTROS, FORS and the reactionless actuator, section 4.3.5 will describe typical available CMGs and reaction wheels, and 4.3.6 will describe typical torque motors.

4.3.2 Fiber Optic Gyros

Fiber optic gyros, [14], are solid-state all-optical inertial detectors with no moving parts. They have the potential to have an automated fabrication process which will make them relatively inexpensive in the long run. All of the optical processing will be on a single chip and the electronics on up to 2 chips. A major technical problem seems to be the attachment of the fibers to the chips. A major expense appears to be in the process of space qualifying the packaging.

FORS, the Fiber Optics Rotation Sensor, is being developed for delivery to Mariner Mark II in 1991. Mariner Mark II development cost is approximately $6.5 million. Upon completion of the Mark II development, additional units are expected to cost less than $1.6 million. For comparison DRIRU II units presently cost approximately $2.1 million. A diagram of an engineering model is shown in Figure 4.3.3.1 [15] and a photo of the engineering model is shown in Figure 4.3.3.2 [15]. Figure 4.3.3.3 [15] displays the FORS random walk performance. Table 4.3.2.1 [15] presents a comparison between FORS and DRIRU II.

An advantage offered by FORS to the Space Station is a much longer lifetime than spun mass gyros. FORS is expected to have a lifetime of greater than 12 years. The performance parameters are listed in Table 4.3.2.2.

Due to their modularity, long life, high accuracy, low mass and power requirements, and anticipated low cost, fiber optic gyros are prime candidates for Space Station inertial sensor.

Table 4.3.1.1
Sensor State of the Art Summary, [9].

SENSOR TYPE	ACCURACY	MASS (kg)	POWER (W)
INERTIAL RATE UNITS		0.2-1.8	0.3-8
GYROS			
1-DOF (HIGH BODY RATES)	0.001 deg/hr		
2-DOF (LOW BODY RATES)	<0.0001 deg/hr		
2-DOF (TURNED ROTOR)	0.001 deg/hr		
2-DOF (MINIATURE TURNED ROTOR)	0.01 deg/hr		
RING LASER (VERY HIGH BODY RATE)	0.007 deg/hr		
FORS (FIBER OPTIC)	0.0001 deg/hr	<10 kg	<10
DRIRU-II	0.00015 deg/hr		
SUN SENSORS			
NULL SEEKERS	$4X10^{-4}$ - $2X10^{-2}$ deg	0.1-7.6	0-15
PULSE GENERATORS	0.2 deg	0.1	0
SOLAR ASPECT	$4X10^{-4}$ - $2X10^{-2}$ deg	0.4-20.7	7-15
EARTH SENSORS			
PULSE GENERATORS	0.1-0.5 deg	0.1-0.2	1
PASSIVE SCANNERS	0.5-3 deg	0.9-11.4	0.5-14
ACTIVE SCANNERS	0.05-0.25 deg	2.7-6.4	7-11
MAGNETOMETERS	1-5 deg	0.9-1.4	2
STAR SENSORS			
GIMBALED TRACKERS	$4X10^{-4}$ - $6X10^{-3}$ deg	14-20	0.4-45
STAR MAPPERS	$5X10^{-4}$ - $8X10^{-3}$ deg	1.1-9	0.5-1.4
FIXED HEAD TRACKERS	$5X10^{-4}$ - $2X10^{-2}$ deg	---	---
ASTROS	$2X10^{-4}$ (GOAL) deg (2.2X2.5 deg FOV)	41	170
PROJECTED CCD ACCURACY YEAR 2000	$1.8X10^{-5}$ (1 deg FOV)		
RELATIVE RATE SENSORS			
TACHOMETER	0.1 % OF OUTPUT	---	---

Table 4.3.2.1
Trade-Off Summary Between FORS and DRIRU II [15]

	IMPLEMENTATION OPTIONS	
FLIGHT UNIT	DRIRU II	FORS
CHARACTERISTICS LONG TERM DRIFT (6 hours) INPUT RATE MASS QUIESCENT POWER POWER AT MAX RATE COST PER UNIT LIFETIME	 0.003°/hr <4°/s 16.9 kg 15 W 23 W $2,100,000 4 years	 <0.003°/hr (GOAL) >100°/s <10 kg <10 W <10 W $1,600,000 > 12 years
ADVANTAGES	ESTABLISHED PRODUCT LOW DRIFT RATE	LONG LIFE LOW RECURRING COSTS LIGHTWEIGHT NO MOVING PARTS LOW MASS, LOW POWER
DISADVANTAGES	MOVING PARTS SHORT LIFETIME	DEVELOPMENTAL PRICE/ PERFORMANCE UNPROVEN

Table 4.3.2.2
Expected FORS Performance [15]

Scale factor stability	10 ppm
Drift	1 microrad/sec over one hr (3 sigma uncompensated)
Max Rotation Rate	4 deg/sec for Mariner Mark II*
Principal error source	optical shot noise (source of random walk)
Pointing Error	0.0001 deg/hr
Expected Lifetime	12 years
Physical Properties	
Mass	less than 10 kg
Volume	less than 0.001 cubic meters
Power	less than 10 watts
Expected delivery date	delivery to Mariner Mark II in 1991
Cost Mariner Mark II development cost approx $6.5M post Mark II - additional units less than $1.6M (DRIRU II - present units approx $2.1M)	
Physical Principles	Sagnac Effect; optical beat detection
Technology Base	solid state integrated optics; optical fiber;
Status	engineering model

(* can be designed for rates greater than 100 deg/sec)

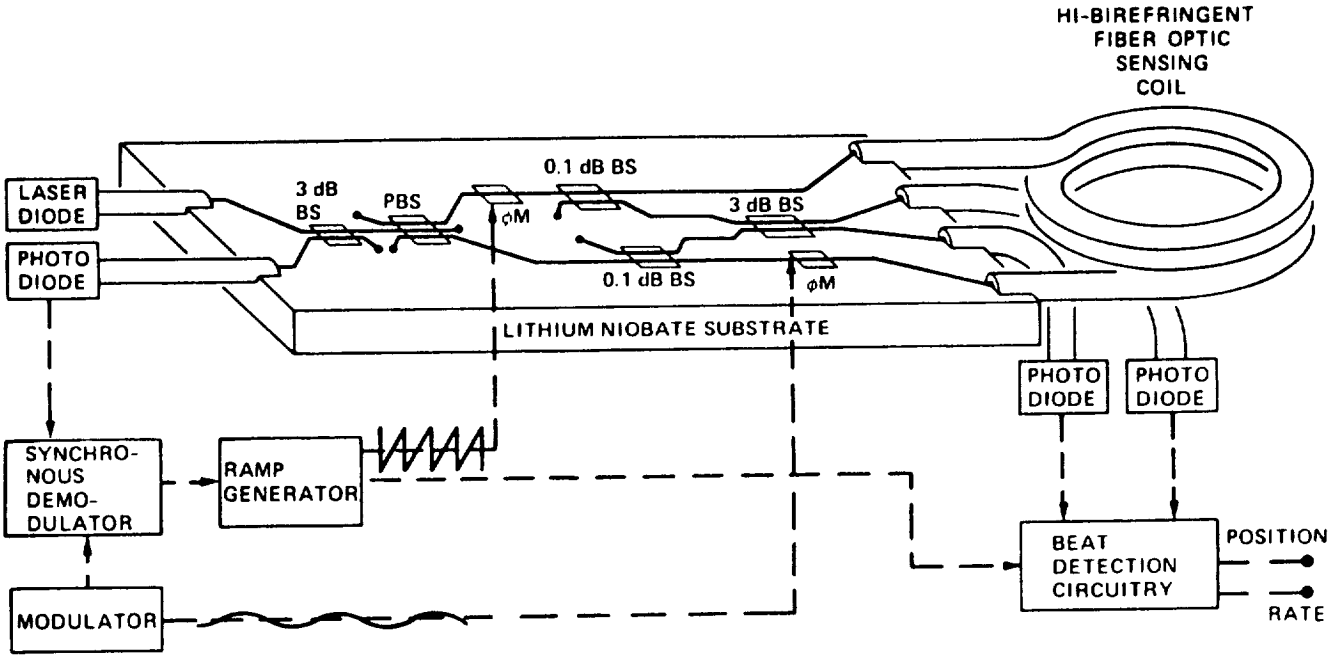

Figure 4.3.2.1
Diagrammatic Representation of FORS [15]

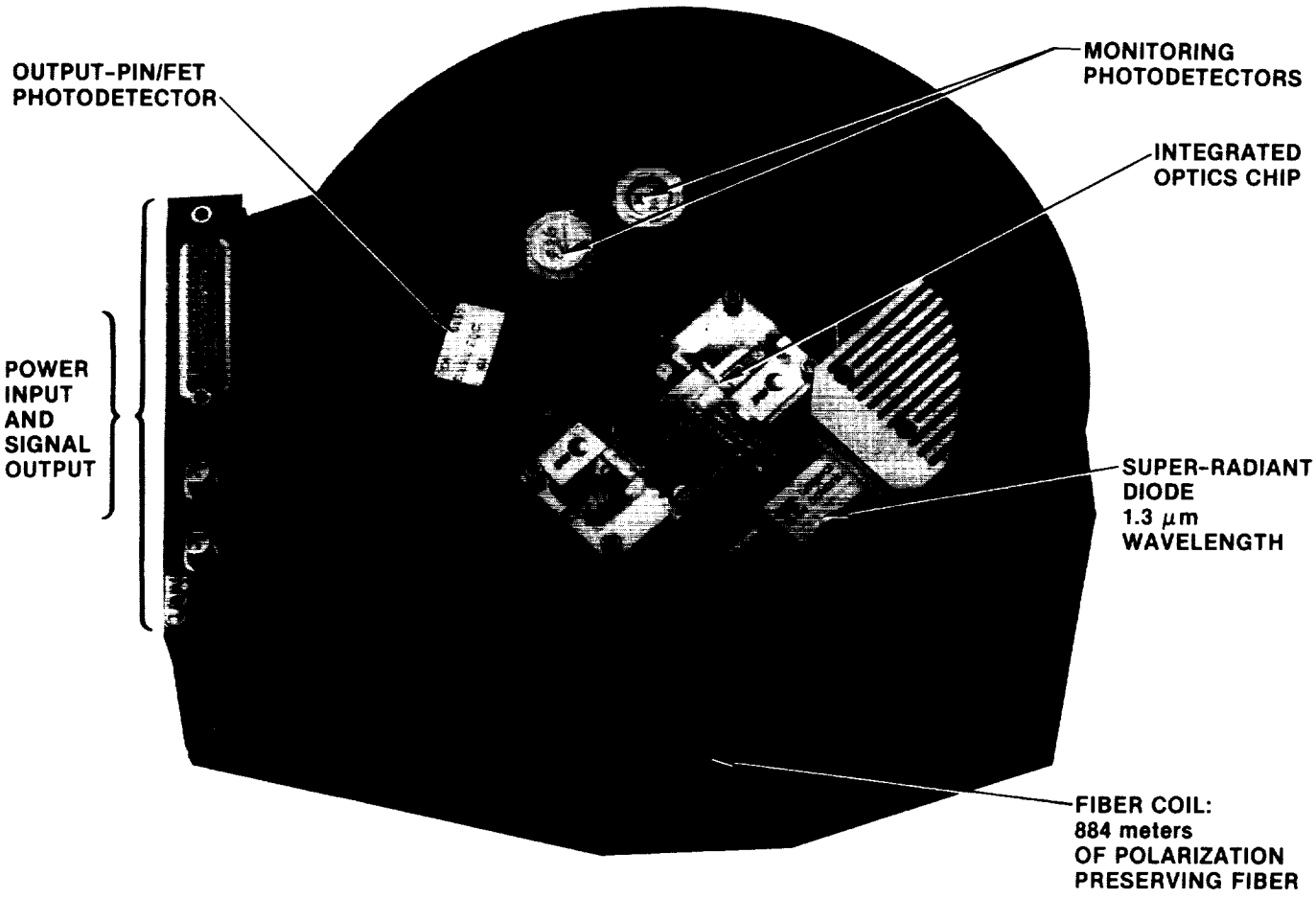

Figure 4.3.2.2
FORS Brassboard [15]

4.3.3 ASTROS: Sub-Arc-Second CCD Star Tracker

ASTROS (Advanced Star and Target Reference Optical Sensor) is a CCD star tracker, [16]. It was designed to provide precise measurements of multiple star image coordinates for input to the image motion compensation system used to stabilize science instrument focal planes. The accuracy of the star location is field of view dependent. ASTROS with a field of view of 2.2 by 2.5 degrees has an accuracy to 0.2 arc-second. Performance tests on real and simulated stars have consistently demonstrated 1/100 pixel accuracy and a noise equivalent angle of 1/300 pixel. The accuracy is star magnitude dependent with dim stars requiring a longer integration time, resulting in reduced accuracy. The thermal/mechanical design has been demonstrated in the laboratory to maintain 0.1 arc-second stability for a low orbit/variable geometry Shuttle mission. Although the large scale pointing accuracy was specified at 4 arc-seconds, achievable large scale pointing accuracy after calibration is expected to be approximately 1 arc-seconds. The ASTROS parameters are listed in Table 4.3.3.1.

ASTROS is designed to measure changes in star position relative to the instrument. The first ASTROS mission was to remove gyro drift errors in an image motion compensation scheme utilizing fast steering mirrors on the Astro payload. ASTROS should not be confused with the name Astro. Astro is the name of an entire payload which has three missions. The principal payload consists of 3 telescopes, but other instruments can be included. Each of the telescopes is attached to an optical bench mounting structure and shares a common bore sight. The optical bench is mounted on the Instrument Pointing System (IPS). The IPS controls the payload line-of-sight (and roll) to any target within approximately 30° of the normal to the Shuttle bay. Most of the base-body (Shuttle) motion is removed by the IPS, providing pointing stability to one of the three principal instruments. The other two instruments require image motion compensation employing articulated secondary mirrors. DRIRU II provides the high-rate-loop error signal to the mirror actuators. ASTROS provides the low-rate-loop error signals to update the gyros relative the payload bore sight. The ASTROS error signal is used to remove the gyro drift error and the structural drifts between the gyros and the telescopes.

ASTROS was delivered for Shuttle launch in March 1986. It is presently awaiting a new launch date. The ASTROS parameters are shown in Table 4.3.3.1.

Table 4.3.3.1
ASTROS Parameters [16]

Position stability	±0.1 arc-sec for 30 min
Noise equivalent angle	0.3 arc-sec (1σ) brightest star in FOV
Small scale accuracy	0.2 arc-sec (1σ) motion up to 10 arcsec
Accuracy	4 arc-sec (1σ) goal 0.8 arc-sec (1σ)
Star acquisition time	< 20 sec
Update rate	> 0.25 Hz
Mass	41 kg
Power	28 V
Electronics	43 W
Heaters	37 W
Radiator system support	90 W
Limited FOV	2.2 X 2.5 degrees
Number of stars tracked	up to 3
Focal length	250 mm
Aperture	100 mm
Magnitude range	-0.8 to 8.2
Integration period	2 to 3900 ms (star brightness dependent)
Status	delivered

4.3.4 Dual Motor Actuator (Reactuator)

Normal actuators provide torque to a gimbaled platform by torquing against the basebody. This torquing induces a rotation of the basebody and excites basebody flexible modes. An inertially reacting design decouples the movement of the gimbals from the basebody by providing torque to a platform without torquing against the basebody. Decoupling the large coarse pointing system from the Space Station would result in a significant reduction of Space Station vibrational disturbance and dynamic interactions.

An implementation of this principle is the reactuator, a dual motor reactionless actuator, [17]. A schematic diagram of the reactuator is shown in Figure 4.3.4.1. This reactuator was designed for the Space Defense Initiative Office Reactuator Gimbal Project at JPL. An engineering model was built and tested in 1987. The device was designed for Shuttle flight.

The gimbal platform, shown in Figure 4.3.4.1, is attached to the basebody through the gimbal bearings. These bearings permit the platform to spin relative to the base. When the top motor in Figure 4.3.4.1 rotates with its flywheel in one direction, the inertial load (platform) spins in the other direction. In a frictionless system, angular momentum would be conserved between the platform and the reaction wheel so that the platform would be moved without any effect on the basebody. Bearing friction and cable torques will, however, couple the platform with the basebody. If only the reaction wheel motor is used, the reaction wheel must speed up in order to oppose these torques and may become saturated in speed. A second smaller motor is added to overcome this difficulty. The second motor shown in Figure 4.3.4.1 replaces the energy lost and prevents speed saturation in the first motor. The second motor ideally exerts a torque equal in magnitude to the bearing friction and cable torque. Thus the reactuator ideally exerts no net torque on the basebody.

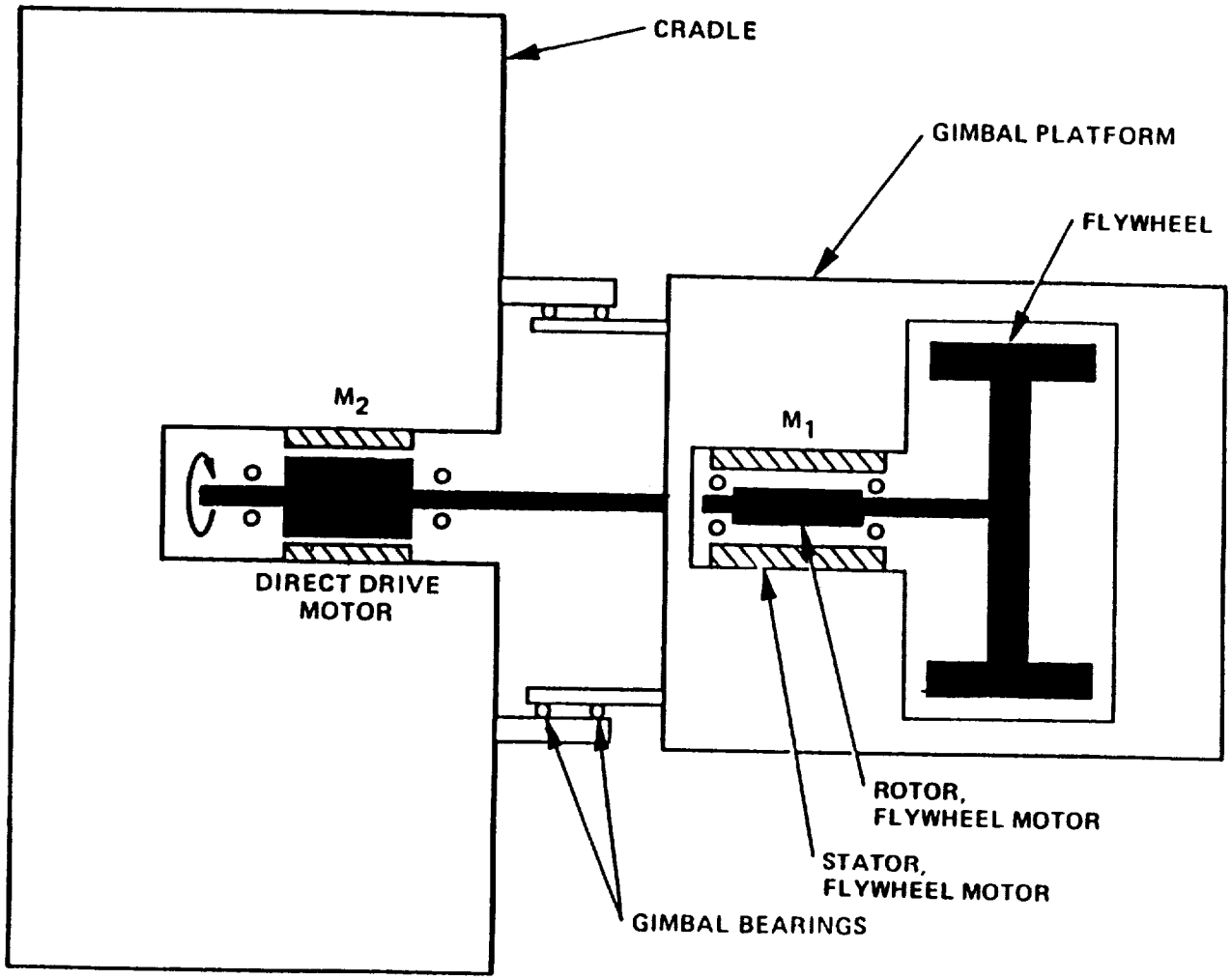

Figure 4.3.4.1
Dual Motor Actuator Diagram [17]

4.3.5 Control Moment Gyros and Reaction Wheels

Four types of actuation are used to control attitude. The four types of actuation are reaction jets, magnetic torquing bars, reaction wheels, and control moment gyros. Each type of actuation has its own limitation. Reaction jets are noisy and unsuitable for the Space Station coarse pointing system. The coarse pointing system reaction jets would have to be independent of the Space Station control system. Reaction jets supply fixed amplitude torques that cannot be torque shaped. They supply fixed amplitude torque impulses that excite the flexible structure modes and degrade precision pointing. Reaction jets require a large amount of fuel for long life actuation. In addition reaction jets present contamination problems. Magnetic torquers can provide only very small amounts of torque. They are both large and heavy. A magnetic field sensor is required. However magnetic torquers may be good for unloading. Reaction wheels require relatively large amounts of power to speed up. Their peak power demands frequently occur at times when power is limited by other demands. Control moment gyroscopes are complex and costly. These limitations are summarized in Table 4.3.5.1, [18].

Reaction wheels and control moment gyros (CMG) are both gyroscopic devices. Spun mass gyros are a well established technology and are expected to improve only marginally on the present state of the art. Ring laser gyros will improve in accuracy to about $1X10^{-3}$ deg/hr by 1990. However, fiber optic gyros are expected to surpass them by 1990. The state of the art (circa 1985) and 1990 projections are listed in Table 4.3.5.2 and shown in Figure 4.3.5.1. The lifetimes of these devices are on the order of 5 to 7 years. However it is expected that space qualified magnetically suspended reaction wheel assemblies, such as the Sperry 1000 foot-pound-second device [19,20], will have longer lifetimes than devices with standard bearings. These devices are modular, and replacement should be simple.

CMGs have the advantage of long life, high torque, low peak power demands, and dynamic range of control authority. There are two types of CMGs, single-gimbal and double-gimbal. Single-gimbal CMGs provide higher torque capabilites than double-gimbal CMGs, and for this reason single gimbal CMGs are usually selected for space applications which require actuator torque greater than 270 N-m. The units shown in Table 4.3.5.3 are present day state of the art in CMGs.

A very large CMG not listed in the table is the Sperry model M4500 [20]. This double-gimbal CMG with 4500 ft-lb-sec (6100 N-m-sec) and an output torque of 200 ft-lb (270 N-m) per axis is the largest double-gimbal CMG made by Sperry.

Another very large CMG is the Bendix [21] model HT-CMG. This CMG has an output torque of 3,400 ft-lbs and a momentum of 1,700 ft-lb-sec. The model HT-CMG weighs 349 pounds. The length along the gimbal axis is 48 inches, and the diameter perpendicular to the gimbal axis is 36 inches. Quiescent power consumption is 74 watts, and the peak

power requirement is 1.2 kilowatts. Spin up time is 5 hours, and maximum burst speed is greater than 11,000 rpm.

Compared to other space programs, the Space Station program coarse pointing system is not expected to make great demands on the state of the art of CMGs. Since it is unlikely that the coarse pointing system will use CMGs for accurate slewing or precision pointing, sufficient capabilities should be provided by the present state of the art. SDI programs, however, can be expected to severely push CMG state of the art. It is expected that, [18], SDI spacecraft will require agile accurate pointing resulting in very large CMGs with low gimbal rate ripple. This expected increase in capabilities may prove useful to the Space Station coarse pointing system. Figure 4.3.5.2 [18] displays Sperry's slew maneuver sizing nomograph for a space-based laser vehicle.

Sperry has projected the following developments in CMGs [18]. Increasing spacecraft size and mass will result in the growth of CMG capabilites. It will be desirable to reduce the size, rotor diameter, and weight of the CMG. Increased rotor speeds from 5,000 50,000 rpm and a reduction of rotor diameter by two thirds are to be expected. This requires changes in rotor materials, and bearing systems. Little improvement is expected in the torquer. It is probable that the electronics assembly modules will be reduced in size and weight or even eliminated by the use of LSI components. With the expected weight reductions and improvements, it is projected that in 25 years, a 300 pound (135 kg) CMG will provide 40,000 ft-lb (54,000 N-m) and 15,000 ft-lb-sec (20,000 N-m-sec) of momentum storage. By comparison, a present day CMG provides an output torque of 3,000 ft-lb (4100 N-m) and 1,700 ft-lb-sec (2300 N-m-sec) momentum storage. The reliability is expected to improve to 98% for 10 years by the turn of the century.

Table 4.3.5.1
Attitude Control Actuator Limitations [18]

ATTITUDE CONTROL ACTUATOR	LIFETIME	TORQUE PEAK POWER	WEIGHT	COMPLEXITY
REAGTION JET	UNLIMITED	HIGH	HIGH	HIGH
MAGNETIC TORQUERS	10/15 yrs	VERY LOW	HIGHEST	MODERATE
REACTION WHEEL	5/10 yrs	LOW	MODERATE	LOW
CONTROL MOMENT GYRO	3/8 yrs	HIGH	HIGH	HIGH

Table 4.3.5.2
Performance/Projection Summary of Reaction Wheels and CMGs. [10]

Type	State of the Art	1990 Projections
Control Moment Gyro 1-DOF 2-DOF	 1-2700 Nms 40-6100 Nms	 ≤4850 ≤12,000
Reaction Wheels	135 Nms (high speed) 50 Nms (medium speed)	550 Nms 200 Nms

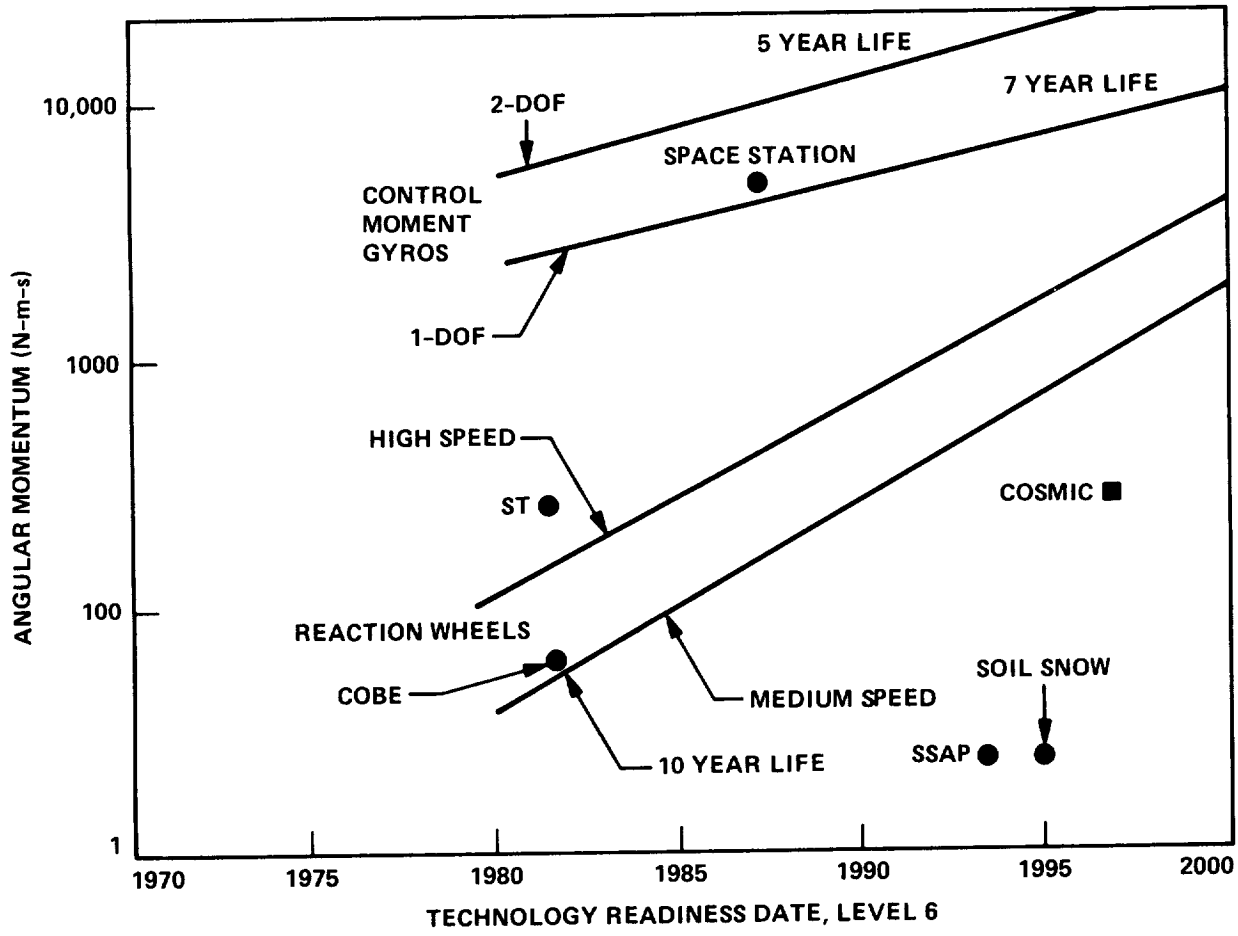

Figure 4.3.5.1
Momentum Wheel Maximum Capabilites Projection [10]

Table 4.3.5.3
Typical State of the Art Sperry CMGs [18]

REQUIREMENT/PARAMETERS	SINGLE-GIMBAL CMG				DOUBLE-GIMBAL CMG
	A	B	C	D	
SELECTION DRIVERS					
MOMENTUM (ft-lb-s)	225	325	1300	1700	325
OUTPUT TORQUE (ft-lb)	225	325	2340	3060	0.7
PEAK POWER (Watts)	140	200	830	613	390
SIZING DRIVERS					
VEHICLE RATE MAXIMUM (deg/s)	.25	.2	6	6.2	0.02
GIMBAL ACCELERATION (rad/s^2)	3	4	5	5	N.S.
RELIABILITY (P_s/YEARS)	.87/7	.96/8	.88/3	.94/3	0.85/5
PERFORMANCE					
BANDWIDTH (Hz)	10	10	20	20	0.17
OUTPUT TORQUE RIPPLE/NOISE(% OF max)	N.S.	N.S.	1.5	0.5	N.S.
OUTPUT TORQUE RESOLUTION (ft-lb)	0.09	0.13	0.3	0.18	0.003
MOMENTUM RESOLUTION (ft-lb-sec)	N.S.	N.S.	21	17	0.28
EMITTED VIBRATION					
ROTOR STATIC BALANCE (lb)	0.9	2.5	0.1	0.1	4.3
ROTOR DYNAMIC BALANCE (in-lb)	9.4	25	1.0	1.0	43
ROTOR AXIAL FORCE (lb)	N.S.	N.S.	1.0	1.0	N.S.
PARAMETERS TO MINIMIZE					
AVERAGE POWER (Watts)	43	75	52	72	110
WEIGHT (lb)	112	144	254	16	155
VOLUME (ft^3) EQUIVALENT CYLINDER	8.4	8.5	22.3	22.3	20

(N.S. = not specified)

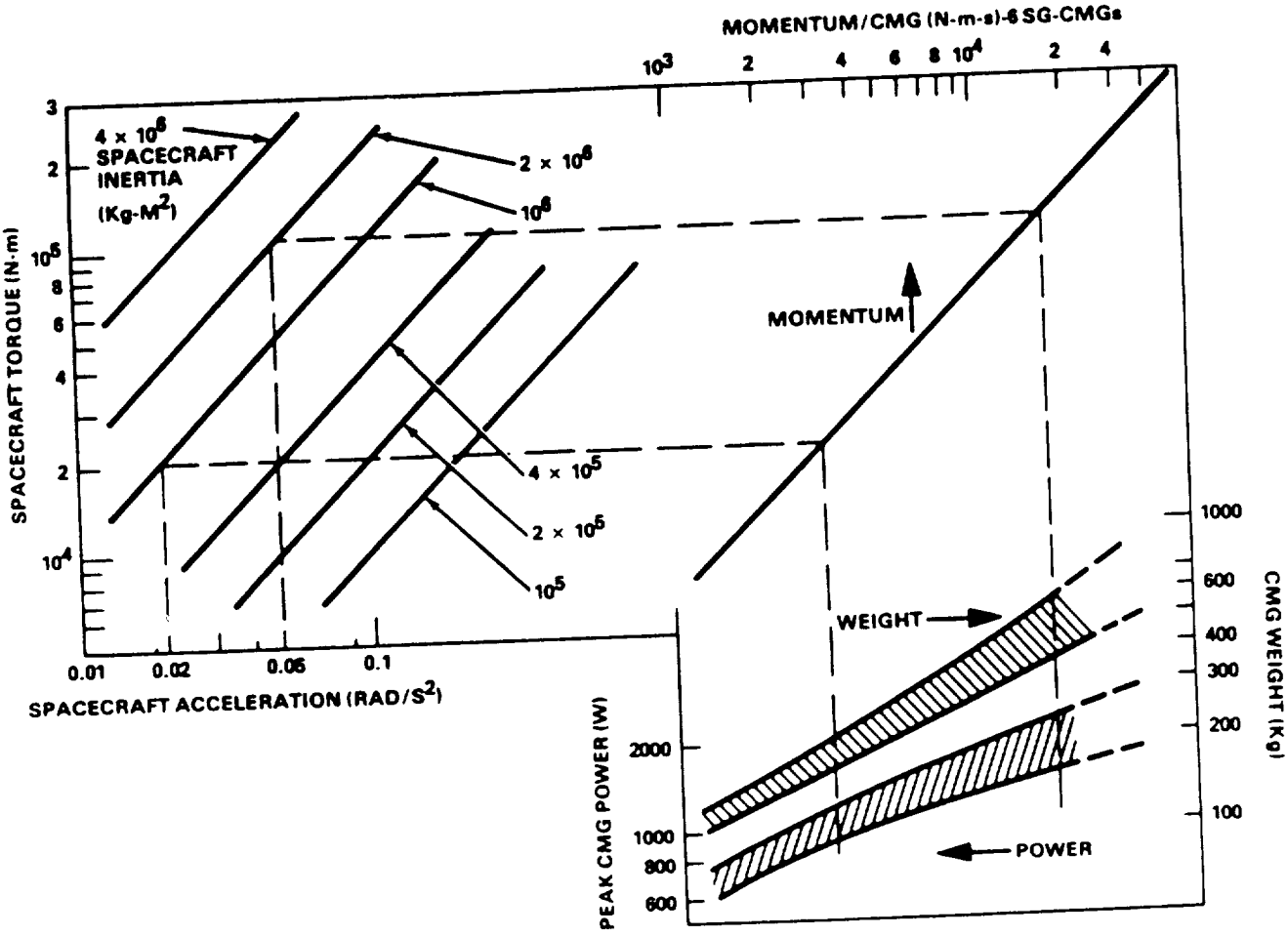

Figure 4.3.5.2
Sizing Nomograph [18]

4.3.6 Torque Motors

Table 4.3.6.1 displays typical torquer motors available from Inland motor company, [22]. Note that QT prefix models utilize rare earth magnets while T prefix models utilize Alnico magnets. Brushless versions of these motors are available. For example, Inland motor 11303B is used on the TAPS gimbal which is to be delivered to GSFC in March 1988. Note that the QT models both weigh less and require less power than the T models. This can be seen by examining the parameters of models QT-12505 and T-12008.

Table 4.3.6.1
Examples of Inland Torque Motors

MODEL	TORQUE (ft-lb)	POWER (watts)	DIMENSIONS (D x L inches)	WT (lb)
QT-11303	100	499	12.2X4.6	39
QT-12505	200	1095	14.0X4.5	67
T-12008	201	2628	16.1X7.5	194
QT-23502	700	1310	25.4X6.0	230
T-24005	1000	7000	30.0X8.0	730
T-36010	1500	4900	41.8X6.8	820
T-18031	1600	5600	23.5X14.8	850
T-36001	3000	6300	41.8X10.2	1360

4.4 Methodology

Central to a pointing system are the control algorithms which receive and process sensors' output data and generate control signals to command torquers to achieve required pointing. As pointing requirements become more and more stringent, the design and development of control algorithms for pointing systems will be compelled to incorporate changes due to three major problems: Coupled dynamics between axes, uncertain flexible dynamics errors, and disturbance rejection.

Dynamic coupling between axes is expected for systems with two or more axis pointing capability, particularly when pointing angle range is large. The classical approach for developing the control algorithms for pointing systems with coupled dynamics is to first ignore the dynamic coupling in the control algorithm designs so that classical single-input-single-output design methods can be used for each axis. The degradation in pointing performance is later assessed or bounded by a simulation with dynamic coupling fully accounted for. This approach has been followed for most spacecraft flown to date.

Modern control methodologies using state-variable descriptions of the coupled system dynamics have been widely reported in the open literature. They include multiple-input-multiple-output (MIMO) design techniques which allow development of pointing control systems that take the coupled dynamics into account. Moreover, the MIMO compensation for a pointing system with coupled dynamics can be designed so the pointing for each axis can be accomplished without disturbing or affecting that of any other axes. This is made possible by decoupling compensation methods. To date, none of the spacecraft pointing systems flown is known to have used the modern methods. However, some of the modern methods are known to have been flight tested on certain space missions.

No pointing and gimbal system is mechanically rigid in an absolute sense. Any body will be seen to be flexible if either very quick or very small motions are observed. Therefore, a pointing system which may be considered rigid for one set of pointing and stability requirements may have to be modeled as flexible if very stringent pointing and stability requirements are imposed.

For flexible pointing systems, the control systems developed from simple classical methods will have a bandwidth which is at least 5 to 10 times lower than the lowest natural frequency of the system, in order to avoid dynamic interaction between the control and the control system. In this approach, performance requirements and the disturbance environment determine the control bandwidth which, in turn, imposes stiffness requirements on the pointing system structure to be built. This philosophy is adapted in most of the spacecraft pointing systems that have been flown to date. In some flight systems, such as missiles which need high pointing performance, the control bandwidth may be close to or even exceed the lowest natural frequency of the structure.

In such circumstances, notch filters have been used to remove certain vibration frequencies from the sensor output so that control commands will not excite those frequencies and cause performance degradation. It is obvious that the effective use of notch filters depends on accurate knowledge of the natural frequencies of the structure.

Modern control methods address the problem of flexible system dynamics by using a large system of equations to represent the system behavior. Currently, MIMO techniques are being developed for flexible systems, and several problems and issues have been identified. The primary problem identified is that there will be both parameter errors and truncation errors in the large system of equations to represent the flexible system. Straight application of MIMO techniques to flexible systems with parameter and truncation model errors can lead to system performance degradation or even system instability. Therefore, current research efforts are focused on three major areas: robust control designs that can tolerate model errors, system identification techniques that can determine system parameters from measurement data, and adaptive controls that provide adequate control performance without having to know the system dynamics a priori.

The performance of a pointing system is critically dependent on its disturbance environment and its disturbance rejection capability. In classical approaches, disturbances are characterized by their power spectral density (PSD). Disturbances are rejected by compensators or filters which are designed based on desired input/output PSD relations. In modern approaches state-space equations may be used to model disturbances, allowing in-flight estimates of disturbances using state estimation or Kalman filtering techniques. Modern approaches have been used to estimate gravity gradient torques, thruster control torques and atmospheric torques on the Space Shuttle. They have also been used for missile guidance and spacecraft orbit determination.

4.5 Image Motion Compensation

4.5.1 Introduction

Many scientific observations require pointing accuracy exceeding the coarse pointing capabilities of the gimbal system on which they are located. The disturbance levels of the basebody, limitations of the coarse pointing system, and slew requirements of the payload seriously limit the pointing accuracy of optical payloads. Pointing requirements can be particularly acute when tracking features on the surface of a planet, satellite, or the sun. It might be expected that a scan platform or gimbal system will be able to continuously point at some surface feature. Due to the large mass of the gimbals or scan platform, movement of the tracking system induces vibrations in the basebody which requires long settling times. To avoid this difficulty, some optical systems are including articulated mirrors in their design. These designs meet image stability requirements by incorporating high bandwidth image motion compensation into the design to remove residual pointing errors of the coarse pointing system. Image motion compensation consists of error sensing and mirror actuation. Usually an inertial detector is used to provide an error signal to the instrument fine pointing control system. If a gyroscope is used and long integration times are required, then gyro drift may become the limiting factor. A star tracker output may be used to provide, based on the star position relative to the tracker, the necessary error signal to the instrument fine pointing control system to remove gyro drift and structure drift relative to the bore sight. The final actuation error signal provided to articulated secondary mirrors is the combination of the gyro error signal and gyro drift error.

Image motion compensation is performed by moving a single mirror. If the mirror system is designed with a second piece, with identical mass properties, which can be moved in the opposite direction, then the system can be made reactionless, [23].

Three image motion compensation strategies will be described. These are the Space Infrared Telescope Facility (SIRTF), the Solar Optical Universal Polarimeter (SOUP), and Ball Brothers fast steering mirror.

4.5.2 SIRTF

Space Infrared Telescope Facility (SIRTF), [24], is a long-life, cryogenically cooled, orbiting infrared observatory which is approximately 1000 times more sensitive than the Infrared Astronomical Satellite (IRAS). To take advantage of this capability, an extremely precise stable pointing and control system is required. SIRTF uses a combination of the spacecraft attitude control system and an actively controlled secondary mirror in the optical train to provide the required image stability and pointing accuracy.

In the dedicated SIRTF spacecraft, control of large and small angle slews, earth-sun-moon avoidance and a first level of disturbance attenuation are provided by the vehicle's attitude control system. Residual motion of the telescope optical axis is removed by a second level of stabilization, active image stabilization. The active image stabilization system utilizes feed-forward from attitude gyros and feedback from the focal plane fine-guidance sensor to drive the telescope's secondary mirror. The pointing performance requirements are for an absolute pointing accuracy of 1 arc-second, image stability of 0.1 arc-second rms. In addition, the spacecraft is required to be able to slew 120 degrees in 8 minutes and have the ability to make small angle slews, up to a maximum of 7 arc-minutes in a time frame of 2 seconds or less. The small slew requirement arises from the need to scan the focal plane over diffuse infrared sources for purposes of mapping. Short slew times are important to maximize the efficient utilization of the cryogen which limits the lifetime of the instrument. If control torques are used for small slews they will produce excitation of structural modes in the basebody. Long settling times, required to allow for damping of these vibrations, will result in loss of cryogen due to pointing at IR sources for unnecessarily long times. Thus the primary design consideration was the need to rapidly execute small angle reorientations of the telescope's optical axis while eliminating settling times. The use of an agile steering mirror eliminates the necessity of using control torques to produce short slews and thus eliminates settling times.

4.5.3 Solar Optical Universal Polarimeter (SOUP)

SOUP, [25], was designed for a 30 cm visible light telescope and focal plane package mounted on IPS on board the Shuttle. Pointing stability requirements were less than 0.05 arc-second jitter over periods of 5 to 20 seconds. This required removal of residual jitter of the IPS and image motion generated on the IPS cruciform instrument support structure. The error signal was provided by solar limb detectors in the prime focal plane. Image motion due to pointing errors was compensated for by an agile secondary mirror mounted on piezoelectric transducers, controlled by a closed-loop servo system.

The fine guider system consists of a set of movable optical sensors, referred to as forks, located at the prime focus of the telescope; processing electronics; and an assembly of piezoelectric transductors which actively tilt the secondary mirror of the telescope. Sunlight enters the telescope, falls on the primary mirror, reflects to the secondary mirror, and reflects to the prime focus where the limb of the sun is detected by the forks. When the system is activated by the dedicated processor, pitch or yaw motion of the prime solar image is detected by the forks. The error signal is sent through the processing electronics to piezoelectric transducers to drive the secondary mirror to remove the motion at the prime focus. Complicated viewing angles require the use of photodiodes to

determine which detector on a fork is to be used in order to maintain an angle of encounter between 90 and 135 degrees.

The secondary mirror actuators are in the mirror's mounting cell, located in the spider of the telescope. The three piezoelectric transducers provide a mirror tilt of 50 arc-seconds by varying the high voltage from 0-1000 volts. The dedicated processor monitors the average voltage and periodically commands the coarse pointer to move a few steps to recenter the secondary mirror.

SOUP assumed an IPS quiescent stability of each axis of 0.75 to 1.50 arc-second rms. Applying the SOUP fine guider to the assumed IPS stability resulted in a residual jitter in line-of-sight of 0.003 to 0.006 arc-second rms for each axis. The transient response was less than 0.03 arc-second peak for an IPS transient of 10 arc-seconds. The long-term guider drift was very much less than solar rotation. Ball has built a small number of these fast steering mirrors, from a 1-inch clear aperture to a 24-inch clear aperture. SOUP flew in July 1985.

4.5.4 Reactionless Fast Steering Mirror

Ball Brothers manufactures a family of two-axis fast steering mirror mechanisms. These are designed to steer a laser beam to its target. A fast steering mirror mechanism contains a mirror and a reaction mass that precisely counterbalances the mirror's movements. Fine pointing and angular isolation are provided by a four-bar linkage with integral spring pivots and linear actuators. Eight voice-coil linear actuators move the mirror and reaction mass. More than 95% of the torque produced in the devices is canceled within the mechanism. The linear range is ± 2 deg with ± 5 deg feasible. Acceleration rates exceed 1000 rad/sec^2. The characteristics of the Ball Brothers family of fast steering mirrors are summarized in table 4.5.4.1. All of the mirrors are characterized by high control bandwidth and small masses. Each mirror has the same range of travel of ± 35 mrad.

Table 4.5.4.1
Ball Brothers Family of Reactionless Fast Steering Mirrors

clear aperture (inches)	control bandwidth (hertz)	pointing resolution (microrad)	pointing linearity (microrad)	tracking accuracy (mrad)	range of travel (mrad)	accel (rad/sec^2)	wt (lb)
1	4000	N.S.	70	25	±35	5000	0.56
2	1000	N.S.	N.S.	80	±35	2600	3
3	650	0.1	12	80	±35	1000	3
5	1000	0.2	8	80	±35	1000	N.S.
6	120	N.S.	N.S.	5000	N.S.	N.S.	N.S.
15	300	N.S.	N.S.	N.S.	N.S.	N.S.	N.S.

(N.S. = not specified)

4.6 Active Thermal Lines/Power Cables Across Gimbals

4.6.1 Thermal Lines

Coolant for payload active cooling can be carried by flexible hoses, but flexible hoses will have the following problems in practical applications: hoses become stiff when pressurized, will restrain range of payload rotation, and the hose material degrades by fatigue and radiation.

Rotary fluid joints allow coolant to flow through gimbals and do not restrain gimbal rotation like hoses do. But the use of rotary fluid joints will require good seal design to prevent coolant from leaking. Moreover, rotary joints still produce substantial friction disturbance torques.

An engineering model for the Talon Gold project was built at Lockheed Missile and Space Company (LMSC) where the rotary fluid joint prototype was tested. The engineering model had a 2.85 cm diameter seal with concentric axial flow paths. The flow rate was 3 gallons per minute of water and ethylene glycol mixture. Heat rejection capability was estimated at approximately 200 watts. Running friction torque was approximately 2.25 N-m, with start-up torque about twice the running value. These friction torques were measured by torque wrenches and therefore, the dynamic characteristics of the friction torques were not available. The results appear highly nonlinear, and will have to be modeled carefully if high pointing performance is to be achieved.

4.6.2 Power Cables

Power and/or data cables crossing the axis of rotation have been modeled as pure springs with non-varying spring constants in the gimbal systems designed and built at Space Data Corporation (SDC). The constant spring model of a cable has resulted in the increased torque ripple due to an extra demand for motor torque. It was also assumed that the spring (i.e., the cable) is restraining the payload in one direction but not in the opposite direction, and therefore, the control design has to accommodate the presence or the absence of the spring. This complicated the control design process, but adequate designs were produced.

In the preliminary design and analysis for the Reactuator Gimbal at Jet Propulsion Laboratory, cable wrap-up torque was modeled by a square hysteresis added with exponential relaxation to represent the basic shape of the twist-flex curve obtained from experimental tests performed to characterize the cable. Figure 4.6.2.1 gives the test result illustrating the twist-flex torque of the cable as a function of its rotation angle. This result was closely simulated with software as shown in Figure 4.6.2.2. Models such as this are required for pushing the control design and predicting the performance of high performance pointing systems.

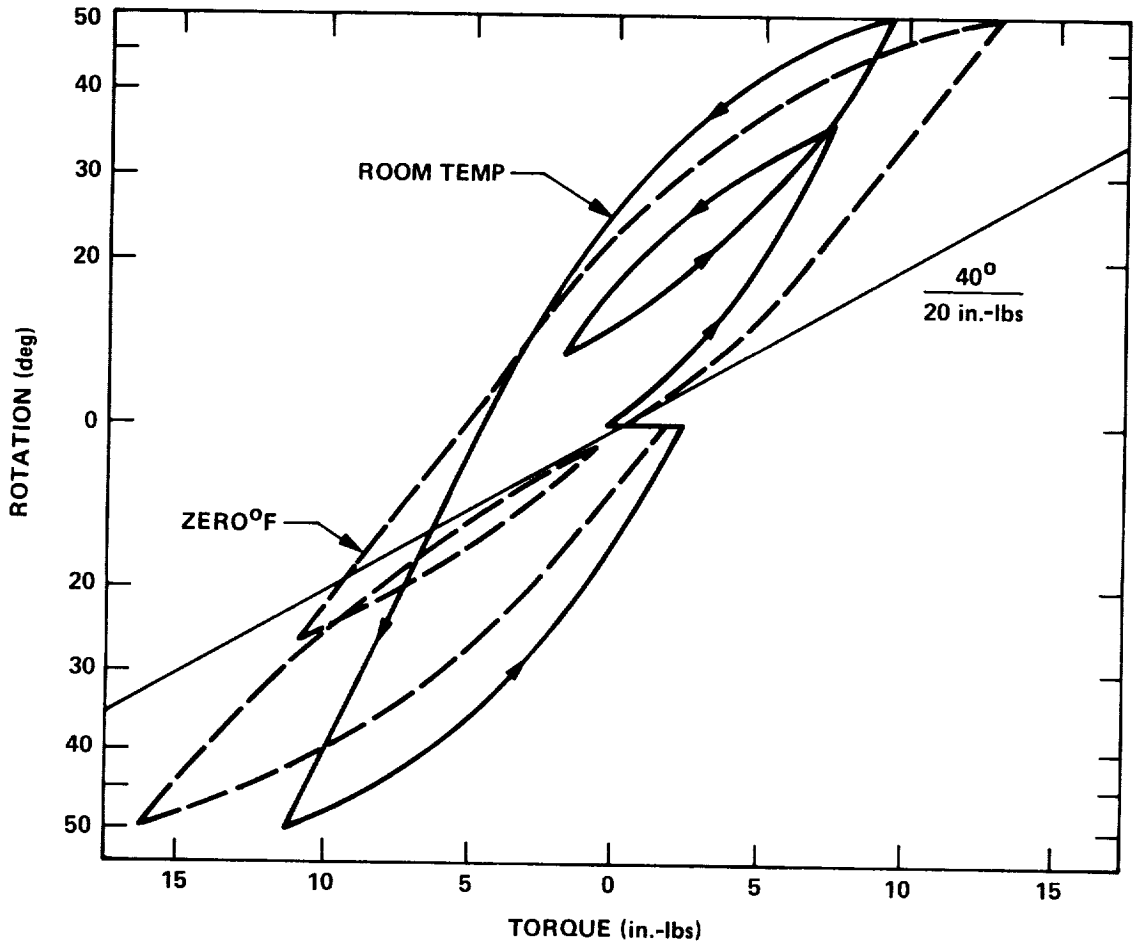

Figure 4.6.2.1
Twist Flex Torque
Test Results for a Reactuator Gimbal Cable

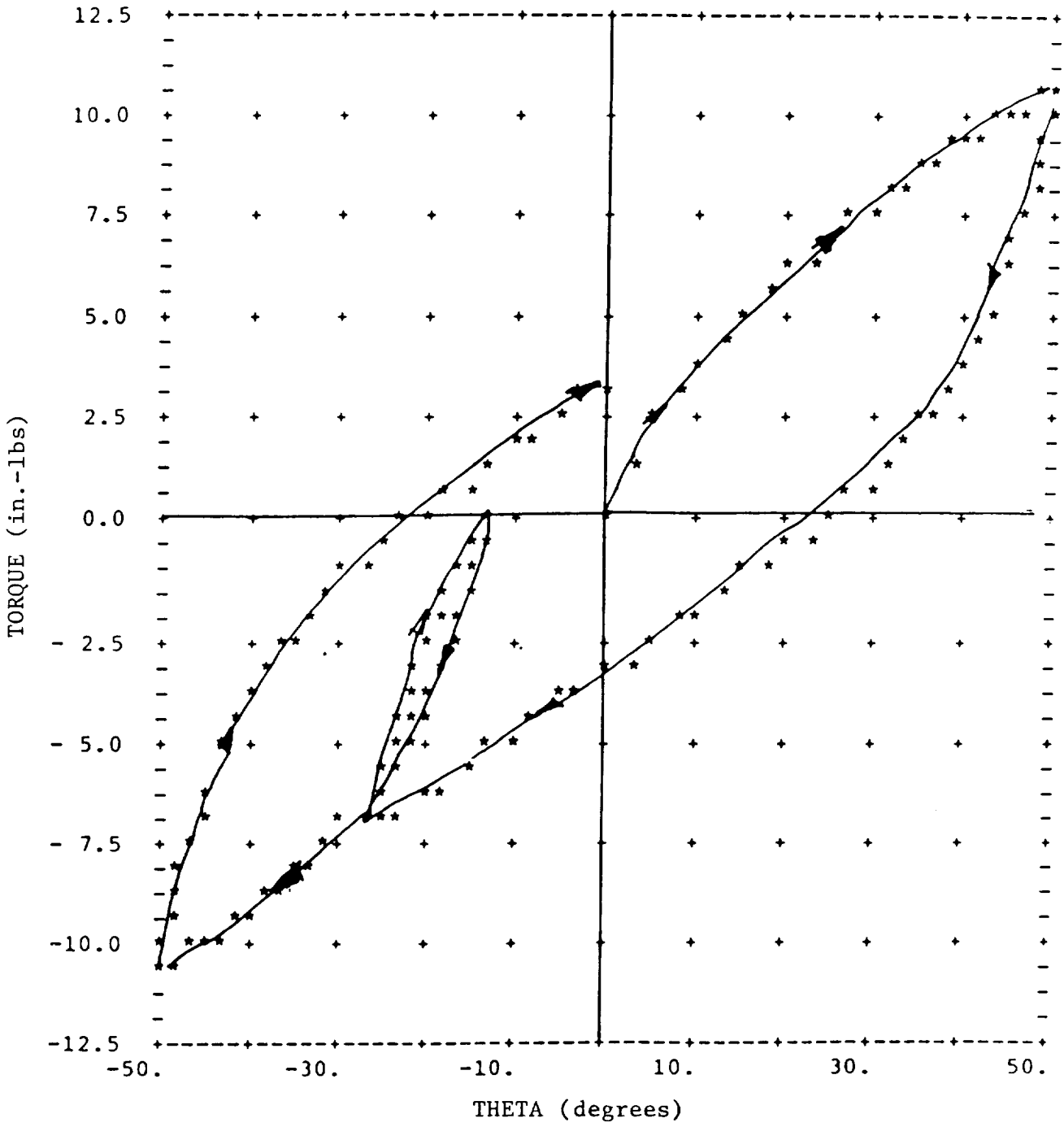

Figure 4.6.2.2
A Typical Simulation Result for the Reactuator Gimbal Cable

4.7 New Materials for Increased Passive Damping

4.7.1 Introduction

The vibrational environment of the Space Station is expected to be substantially dirtier than the Shuttle. In order for the coarse pointing system to meet its pointing requirements, it is anticipated that active and passive damping control will be required. Passive damping can be incorporated into the design of the coarse pointing system and its interface structure to the Space Station. Incorporation of passive damping through utilization of structural materials with high damping parameters and viscoelastic materials for additional damping will result in improved dynamic stability and performance of the system and, potentially, in an active control system which is lower in cost, weight and complexity, [26, 27].

Passive damping can be introduced in two ways: using structural materials to dissipate vibrational energy and using discrete dampers (dash pots, internal surface layers, absorbing foam cores). The damping properties of various materials and their limitations for space applications are discussed in the following sections.

There are four categories of materials to consider:

1. structural metals and alloys
2. viscoelastic materials
3. polymer matrix composites
4. metal matrix composites

Tables are provided for each type of material. These tables show typical materials and parameter values.

4.7.2 Space Environmental Conditions

The harsh space environment imposes unique difficulties for some of the damping materials such as viscoelastic and polymer matrix composites which exhibit outgassing [27].

1. The high vacuum of space results in a serious outgassing problem for many damping materials that cannot be tolerated. Outgassing changes the physical properties of some materials so that they lose their damping properties. In addition the Space Station contamination requirements impose strict limits on outgassing. Thus many damping materials will have to be encapsulated to prevent outgassing in order to stay within Space Station contamination bounds and to retain their damping properties. Even encapsulation is not a complete solution to the outgassing problem. High velocity micro-meteorites will penetrate the encapsulation layers causing holes. Even small holes will allow outgassing which could easily exceed Space Station outgassing limits. Encapsulation may be limited to thick walled dash pots.

2. Thermal fluctuations (-250°F to 250°F) in space are much larger than the temperature range in which many materials exhibit damping. Viscoelastic materials have poor damping properties at low temperatures. Use of damping materials will probably require active thermal control.

3. The radiations, both electromagnetic and particle, present in the space environment induce changes in some materials which reduce their effective damping properties. Encapsulation may eliminate this problem.

4.7.3 Loss Factor

The damping characteristics of the materials are presented in terms of the loss factor. For low damping levels, the loss factor, eta, equals twice the damping ratio.

4.7.4 Structural Metals and Alloys

Table 4.7.4.1 lists loss factor values of various structural alloys at room temperature and low stress levels. Damping at low stress or strain levels is independent of stress or strain amplitude and varies with frequency and temperature. Conventional aluminum and titanium base structural alloys exhibit low damping. From inspection of Table 4.7.4.1, it is observed that the loss factor is highest for copper manganese alloys, nitinol and ferromagnetic materials. However these materials all possess high densities and cannot be recommended for space applications because of weight penalties. It is possible to use them in metal matrix composites by incorporation in the matrix material. Cast magnesium is an exception and is a potential candidate for space gimbals.

Table 4.7.4.1
Damping Properties of Structural Alloys [27]

Material	Loss Factor	Freq. Range
2024 T-3 Al	$2.4X10^{-3}$	10-100 Hz
6061 T-6 Al	$2.0X10^{-3}$	10-100 Hz
1020 Steel	$5.0X10^{-4}$	50-500 Hz
Ti-6Al-4V	$2.0X10^{-4}$	@ 40 kHz
310 Steel	$1.0X10^{-3}$	kHz range
403 SS	$1.4X10^{-2}$	" "
Brass	$9.0X10^{-2}$	" "
NIVOC	$3.0X10^{-2}$	" "
Nitinol (Ni-45 Ti)	$2.8X10^{-2}$	" "
Sonoston (Mn-36Cu 4.5Al 2Ni 3Fe)	$4.0X10^{-2}$	" "
Cast Iron (coarse graphite flake)	$5.7X10^{-2}$	" "
Fe-12 Cr-3 Al	$3.6X10^{-2}$	" "
Incramute (Cu-44Mn 1.8 Al)	$3.1X10^{-2}$	" "
Cast Pure Mg	$3.9X10^{-2}$	" "

4.7.5 Viscoelastic Materials

Table 4.7.5.1 lists peak loss factor values of a few viscoelastic materials and their effective temperature range at 100 hertz.

From inspection of Table 4.7.5.1, it is seen that viscoelastic materials exhibit very high damping compared to structural alloys. However their capacity to dissipate vibrational energy occurs in a narrow temperature range and is strongly influenced by frequency. Viscoelastic materials exhibit poor damping at low temperatures. Space environmental factors of outgassing, irradiation and low temperatures severely affect damping properties.

Because of their very high loss factor, it is very desirable to use viscoelastic materials if their inherent limitations can be overcome. Three candidate methods are [27]:

1. encapsulated discrete dampers
2. acrylic core foam in hollow structures such as struts or gimbals
3. encapsulated viscoelastic layer on interior surfaces

However, active thermal control may be required to keep the material within their effective temperature ranges.

Table 4.7.5.1
Damping Properties of Viscoelastic Materials [27]

	@ 100 Hz				Effective Temp °F	
Material	Density lb/in^3	Temp °F	Peak loss Factor	Modulus psi	min	max
113 (3M)	.0380	0	1.20	$1.0x10^3$	-15	45
ISD 113 (3M)	.0340	19	1.50	$4.0x10^2$	-25	20
ISD 110 (3M)	.0348	145	1.25	$3.5x10^3$	125	10
Acrylic Core Foam (3M)	.0210	85	1.20	$5.0x10^2$	35	135
DYAD (606) (Soundcoat)	.0350	105	1.00	$3.5x10^3$	98	143
Soundcoat M (Soundcoat)	.0370	90	1.50	$7.3x10^2$	50	135
Soundcoat N (Soundcoat)	.0620	38	1.40	$4.5x10^6$	5	100
SMRD-100-F90 (GE)	.0256	80	0.90	$6.0x10^3$	70	95
IF2012 (Morgan Adhesive)	.0348	62	2.00	$5.5x10^1$	8	225
National TM119 (National Starch & Chem)	.0360	75	1.50	$5.0x10^1$	50	115
Plexiglass		70	0.085	$5.3x10^5$		
Lexan		70	0.010	$3.3x10^5$		

4.7.6 Polymer Matrix Composites

Table 4.7.6.1 lists typical loss factors of fiber reinforced polymer matrix composites. Extensive R&D effort on polymer matrix composites is being expended under the auspices of Wright Patterson Aeronautical Laboratory at Wright Patterson Air Force Base [26]. The purpose is to identify structural materials for space structures which exhibit higher damping and stiffness to density ratio than conventional aluminum and titanium base structural alloys.

From inspection of Table 4.7.6.1 it is seen that polymer matrix composites exhibit greater damping than conventional aluminum and titanium base structural alloys. Their limitations are the same as viscoelastic materials. Exposure of the matrix to space environmental conditions of high vacuum, radiation and thermal cycling results in outgassing, and material degradation with decreases in damping, particularly at low temperatures.

Table 4.7.6.1
Damping Properties of Polymer Matrix Composites [27]

Material	Peak Loss Factor	Comments
Gr/epoxy (0)	$1.28X10^{-3}$	40-140Hz (@$700x10^{-6}$)
Gr/epoxy (90)	$1.10X10^{-2}$	" "
Gr/epoxy ($\pm$45)	$1.10X10^{-2}$	" "
Kevlar/epoxy	$2.00X10^{-2}$	" "
HT-S/epoxy-F	$3.80X10^{-4}$	" "
HT-S/epoxy-Ly	$4.00X10^{-4}$	" "
E glass/epoxy Dx21	$1.75X10^{-3}$	" "
Gr/epoxy (1/d $\triangleq$ 20) (predicted)	$2.80X10^{-2}$	" "
Gr/epoxy (1/d $\triangleq$ 200)	$0.80X10^{-2}$	" "

4.7.7 Metal Matrix Composites

Table 4.7.7.1 lists typical loss factors of metal matrix composites. From the inspection of Table 4.7.7.1, it is seen that metal matrix composites exhibit about the same loss factors as the polymer matrix composites but greater loss factors than conventional aluminum and titanium base structural alloys. They do not have the space environmental limitations of the polymer matrix composites of outgassing, radiation degradation and poor damping at low temperatures.

The difficulties associated with metal matrix composites are related to fabrication (voids, delamination, fiber twist and alignment, and residual stress), cost and the immaturity of the technology. Metal matrix composites present a difficulty in that they cannot be modified after they have been fabricated. Thus for example post fabrication holes cannot be drilled in order to make new attachments. They are however excellent candidates for structural materials for use in connecting the coarse pointing structure to the Space Station (station interface assembly) where the structure design will be well known.

Figure 4.7.7.1 displays the damping behavior of P55Gr/60661Al composites [27]. Like metallic materials, damping in metal matrix composites varies with vibration strain amplitude. At low strain amplitude levels $< 10^{-5}$, the specific damping capacity of Gr/Al composites is nearly independent of dynamic strain, but lower than the damping value of aluminum matrix. At intermediate strain levels, damping capacity increased with an increase in strain until it passed the value for aluminum. In addition to Gr/Al, cast Gr/Mg - 1% Zr and Gr/Mg - 1% Mn composites with optimal microstructures have the potential to exhibit high damping.

Table 4.7.7.1
Damping Properties of Metal Matrix Composites [27]

Material	Loss Factor	Comments
B/Al [0°]	$1.5\text{x}10^{-2}$	@ freq. 2000 Hz/450°C
P100 Gr/Al [0°]	$4\text{x}10^{-3}$-$9.00\text{x}10^{-3}$	@ freq. 40 Hz/25°C
P100 Gr/Al [90°]	$2.40\text{x}10^{-2}$	"
B/Al [0°]	$5.0\text{x}10^{-3}$	@ freq. 1 Hz/20°C
P100 Gr/Mg [0°]	$2\text{x}10^{-3}$-$1.2\text{x}10^{-2}$	@ freq. 40 Hz/25°C
P100 Gr/Mg [90°]	$1.80\text{x}10^{-2}$	"
20/SiCw/Al	$1.48\text{x}10^{-3}$	"
P55 Gr/Al [0°]	$4\text{x}10^{-3}$	@ freq. 0.1 - 10 Hz/25°C
Gr/Mg - 1% Si	$8.0\text{x}10^{-3}$	

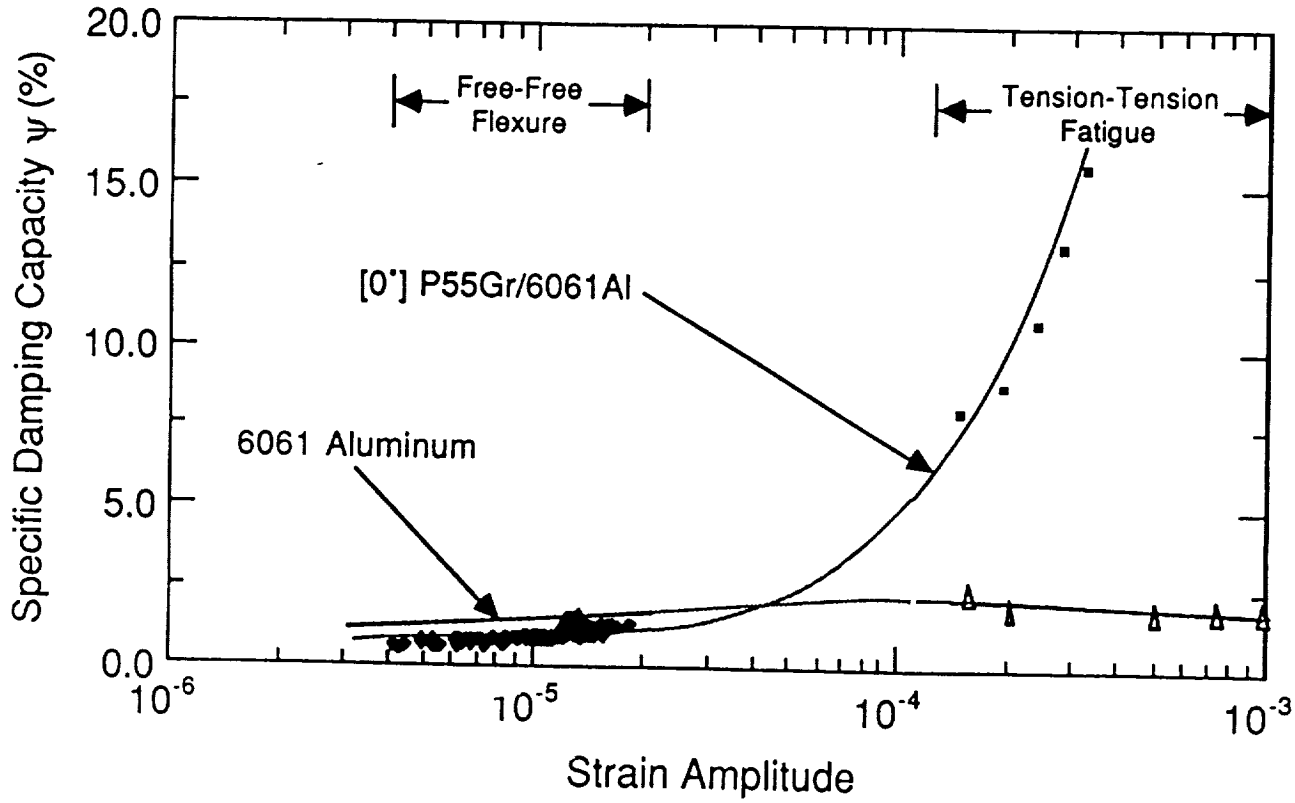

Figure 4.7.7.1
Damping Behavior of P55GR/60661AL Composites [28]

4.7.8 Summary and Recommendations

Passive damping can only provide on the order of 1 to 2 percent damping. However incorporation of passive damping into the design of the coarse pointing system, particularly into the coarse pointing system Space Station interface assembly structure, which connects the coarse pointing system and the Space Station, should not be ignored. Use of structural materials with better damping properties, viscoelastic layers, and discrete dampers will improve the dynamic stability of the system and result in improved vibration control and performance, specifically for low amplitude vibrations if they can be incorporated into the design.

For viscoelastic materials and possibly polymer matrix composites, the space environment results in problems with outgassing, material degradation due to both outgassing and irradiation, thermal cycling, and temperatures outside the normal damping region. These limitations result in a pessimistic view of the use of many damping materials in space. Metal matrix composites do not have all of these limitations but appear to still be in the R&D phase and to have the problems associated with this phase of high cost and difficulties in reliable fabrication.

4.8 Tethered Pointing Platform/Payload

Tethered operations in space have been considered in a number of previous missions, e.g., Orbiting Astronomical Observatory and Lunar Module/Apollo Telescope Mount. Since 1984, there has been renewed interest in tethered pointing platforms or payloads for flight test with the Shuttle and for applications with the Space Station [29].

Tethered pointing platforms or payloads connected to the Space Station will have the benefit of being isolated from Station dynamic disturbances. If the tether is long enough, the platform or payload can avoid contamination from Station exhausts. Yet the platform or payload is close enough to the Station that rapid retrieval from the Station and use of Station utilities are possible. However, operation difficulties and technical problems are also introduced by tethering a platform or payload to the Station. For example, the deployment and the retrieval of tethered platforms or payloads has not been done before, and tethered operations must be performed in such a manner that the safety of the Station is ensured. To assure safety, tether dynamics must be understood completely so that the swing motion of the tethered platform remains within acceptable limits when the platform is reeled in and out. Tether materials must also remain strong enough in the presence of micro-meteorite impacts, electromagnetic radiation, and thermal cycling.

Tension along the tether can be used to control and stabilize the attitude of the tethered platform or payload, if the tether attachment point is made movable. For example, Figure 4.8.1 [30] shows mechanism concepts for moving the tether attachment point so that the tether tension does not go through the center of mass of the platform or payload. This permits creating a control torque from the gravity force and the tether tension. This control torque can be effective in controlling pitch and roll of the pointing platform or payload. If the attachment point can be controlled precisely, the stability of the platform or payload can be controlled to a few arc-seconds.

In 1985, AERITALIA of Italy reported a simulation result [31] on the performance of a tethered pointing platform in which tether librations and the first two longitudinal vibrations were included in the dynamic model. Assuming perfect sensors and actuators, the attitude accuracy achievable was in the sub-arc-second levels. The movement required of the attachment point, to achieve this accuracy, was less than a few millimeters.

In fact, the pointing control concept by movable attachment point was first proposed in 1984 by L. Lemke of Ames Research Center who also proposed a Shuttle tethered flight experiment, Kinetic Isolation Tether Experiment or KITE. As shown in Figure 4.8.2 a low-cost spacecraft such as Spartan is tethered to the Shuttle in the proposed KITE concept. Tether length is from 1 Km to 5 Km. A single degree of freedom laboratory model has been developed that demonstrated a pointing accuracy in the arc-second range. Hardware development for the flight test is still being planned for a 1989 start.

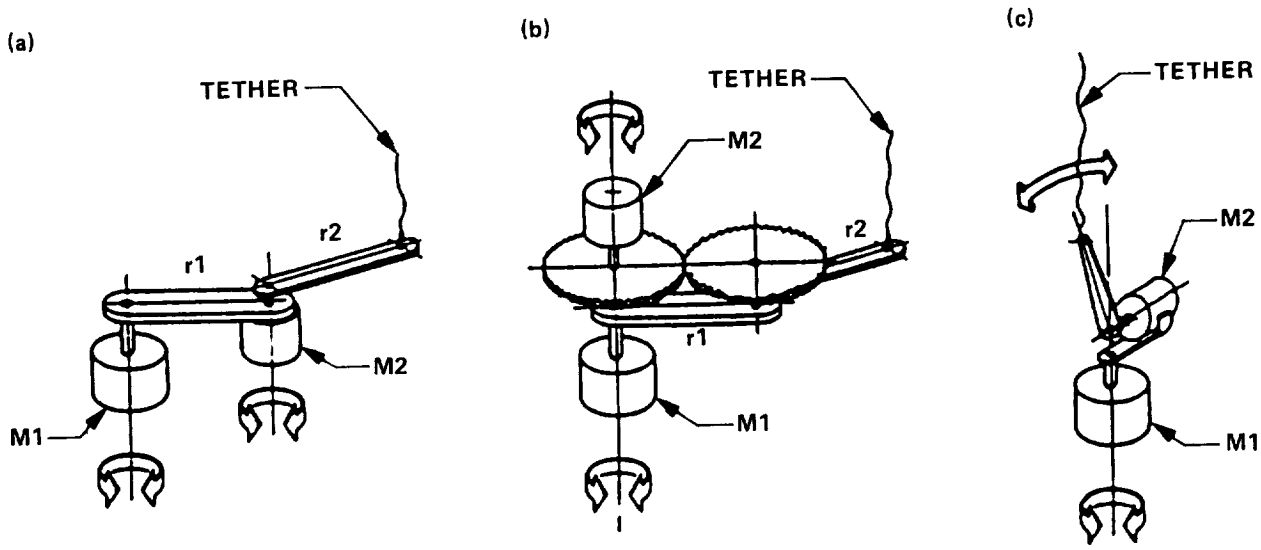

Figure 4.8.1
Mechanism Concepts for a Movable Attachment Point [30]

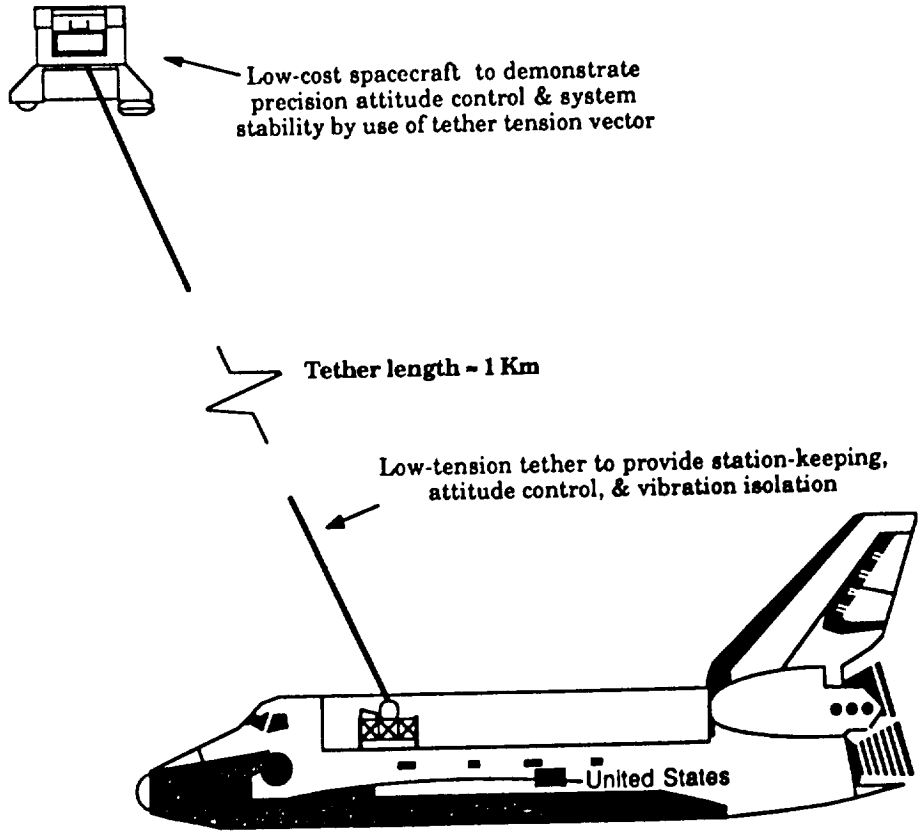

Figure 4.8.2
Kinetic Isolation Tether Experiment Concept [32]

4.9 Softmounted Inertially Reacting Pointing Systems

4.9.1 Introduction

An alternative to the simple gimbal approach to pointing systems arises from consideration of both adding a low pass filter between the basebody and the payload, and mounting the payload on its own free flying spacecraft. Consider the system architecture depicted in Figure 4.9.1.1. The mechanically "hard" gimbal is replaced by a very "soft" interface which is largely passive but must have at least an intermittent active mode which allows it to reposition the payload in a gross fashion and latch it up to the base vehicle if necessary. During normal operations the "softmount" acts as a low pass filter that sets the cut-off frequency as low as is practically possible. In the limit, as mount stiffness goes to zero, the payload is free flying in tandem with the base vehicle. The pointing control resides on board the payload side of the mount where inertially reacting actuators such as reaction wheels or CMGs implement the high bandwidth disturbance filtering and tracking/slewing control. In actuality, the controller on board the payload is not bandwidth limited by basebody flexibility, since control torques are not generated by reaction against a relatively flexible base vehicle, but against a relatively rigid spinning wheel. Notice that this concept is fundamentally different than an isolation system between the base vehicle and a gimbal which is sometimes referred to as a softmount. Such a system must still pass the basebody reaction torques that allow the payload to be articulated. The stiffness of such a system is tightly constrained by the competing interests of disturbance isolation and slew response.

A softmounted inertially reacting pointing system architecture may be implemented in many ways. Any one of the available vibration isolation techniques may be used; however, those that allow only limited travel (such as flexure or magnetic suspension systems) will need a gimbal stage, possibly using an inertially reacting system such as the reactuator. One softmount design that allows large relative motion using a "solid state" softmount design is described below.

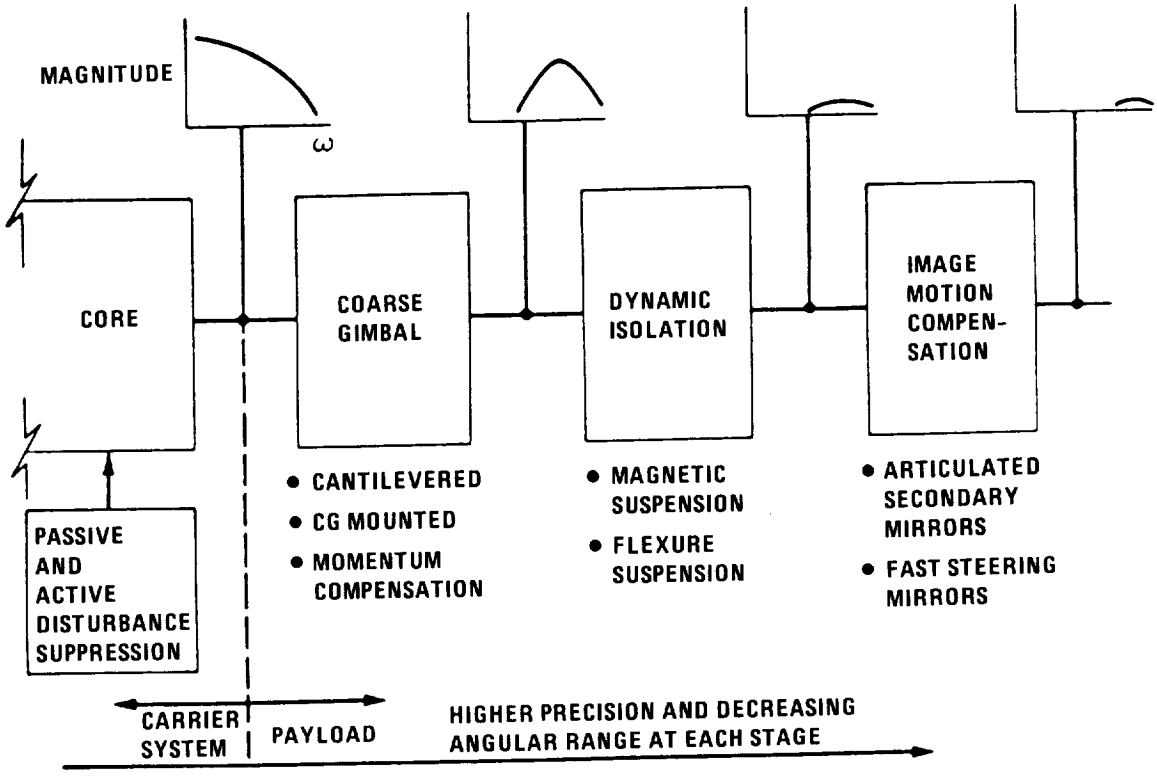

Figure 4.9.1.1
Multi-level Actuation Architecture.

4.9.2 Piezoelectric Polymer (PVF_2) Softmount Design

A diagram of the softmounted inertially reacting pointing system (SIRPNT) is shown in Figure 4.9.2.1. SIRPNT's key element is the all solid state PVF_2 active softmount. This softmount consists of two or more nodes arranged in an alternating pattern as depicted in the Figure. The softmount is intended to conform to the arbitrary motions of both the payload and the base vehicle, and to do so in such a way as to present the lowest possible stiffness. In fact, due to the reciprocity between electric field and strain in piezoelectric materials, if an imposed deformation gives rise to an electric field in the material, then external application of that same field would induce strains that would exactly mimic the imposed deformation. This property can be used to actively cancel any residual stiffness of the softmount. The material is sufficiently flexible itself to provide substantial vibration isolation however. Thus, the active control may be used to obtain desired damping characteristics or to reduce the effects of other stiffnesses present, such as power and data cables, as well as to provide translational station keeping of the payload with respect to the base vehicle.

The structure of a single node is also depicted in Figure 4.9.2.1. It consists of two or more laminated sheets of PVF_2 film, nominally semicircles in cross section, whose upper and lower edges are cantilevered into the nodal end plates. As shown, the node is soft in five degrees of freedom and hence capable of actuation in the same five degrees of freedom. The only stiff degree of freedom is along the translational axis that runs between the two PVF_2 sheets. Hence by stacking the nodes such that this stiff axis is staggered by 90 degrees, a full six degree of freedom softmount can be achieved with two nodes. Additional nodes amplify the possible relative deflections between the basebody and the payload.

Running through the center of each nodal end plate is an inflatable tube that forms the core of the softmount. This tube, which is nominally not inflated and hence slack, can contain the power and data wiring running from the basebody to the payload. It is inflated only as a fail-safe means of introducing required stiffness in the event of an electrical failure of the softmount. It might also be used in the deployment and retrieval process.

Since the PVF_2 material is the key element of this softmount design, a brief discussion of the properties of PVF_2 and its utilization in the "bimorph" configuration is in order. Poly (vinylidene fluoride) is a relatively new piezoelectric substance which saw its first use and early characterization in Japan in the 1960s [33,34]. It has only recently come to widespread attention in this country [35,36]. However, it is now in commercial production in the U.S. under the trade name Kynar [37] and is being used in a variety of transducer applications. Many of these applications stem from the fact that PVF_2 is flexible, lightweight, and is readily manufactured in sheet form. This is in contrast with more conventional piezoelectric ceramic

materials which are generally brittle, heavy, and difficult to manufacture and customize. Other significant properties of PVF_2 include: high piezoelectric sensitivity, extremely good frequency response, high dielectric strength, high operating field strength (30 times higher than ceramics), resistance to hostile environments, and availability as large area thin film that is readily cut and shaped to form complex configurations, easily laminated to produce bimorph and multimorph elements that multiply transducer response. When subjected to mechanical impact, it is resistant to breakage and loss of dipolar properties. PVF_2 has flown in space both on the Space Shuttle and on the Soviet Vega spacecraft which flew by Halley's Comet [38]. In both instances, however, it was used in one of its sensing modes. It has not been used in space to date as an actuator.

The use of PVF_2 as an actuator stems from the fact that when an electric field is introduced across a sample of the material, a local strain is induced. This strain is primarily in one of the directions orthogonal to the applied field. A "bimorph" actuator can be created by bonding two sheets of PVF_2 together and introducing oppositely directed electric fields across them. This causes one of the sheets to contract while the other expands, leading the bimorph to bend as would a bimetallic strip in a thermostat. This effect is illustrated in Figure 4.9.2.2. Building sheets of PVF_2 into bimorphs greatly multiplies the field induced displacements that can be achieved. Multimorphing, i.e., building multi-layer bimorphs, allows the ratio between field induced displacements and field induced forces to be adjusted. The SIRPNT design uses multimorphs built up out of layers whose metallization surfaces have been etched, so that the surface is divided into various regions which may have different voltages. Shaping the distribution of voltage across the surface allows the shape of the multimorph to be controlled.

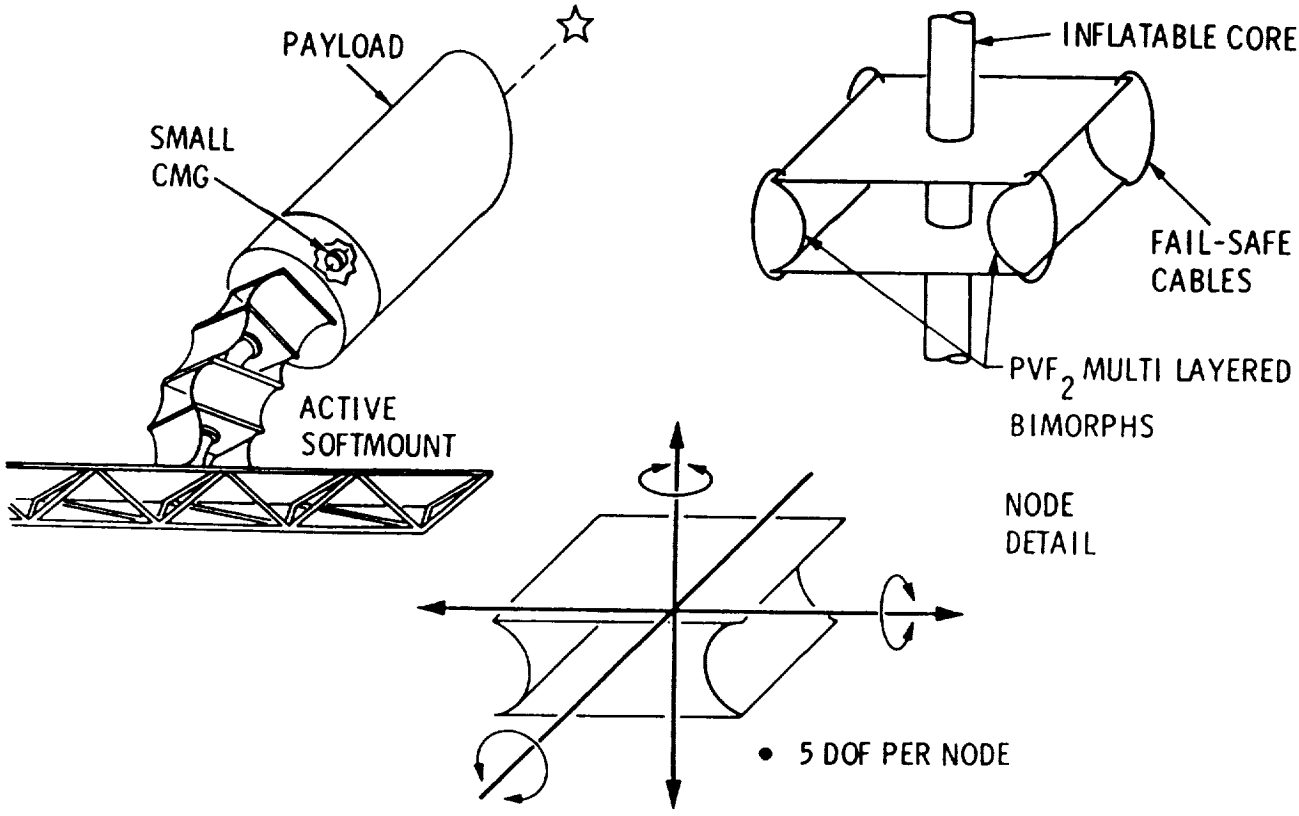

Figure 4.9.2.1
SIRPNT PVF_2 Design Concept

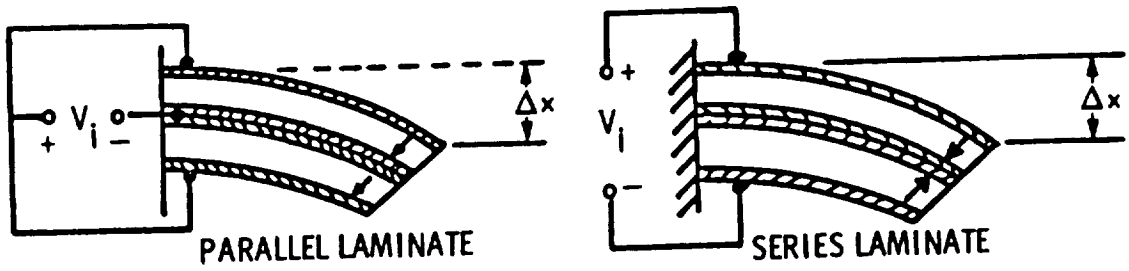

TIP DISPLACEMENT

$$\Delta x = \frac{3}{4} \frac{V d L^2}{t^2}$$

TIP FORCE GENERATED

$$F = \frac{3}{2} \frac{V d E b t}{L}$$

MULTIPLE LAYER PAIRS

$$\Delta x = \frac{3 L^2 d \ V}{4 n t^2}$$

$$F = \frac{3}{2} \frac{V d E b t n^2}{L}$$

V - APPLIED VOLTAGE
d - PIEZOELECTRIC STRAIN CONSTANT
L - BIMORPH LENGTH
t - LAYER THICKNESS

E - YOUNG'S MODULUS
b - BIMORPH WIDTH
n - NUMBER OF BIMORPHS

Figure 4.9.2.2
PVF_2 Bimorph Characteristics

4.9.3 Softmount Architecture Advantages

The softmount architecture considered here offers the following advantages over the more traditional gimbal based options:

1. Potential for High Performance -- since, in the limit, the payload becomes a free-flyer, accuracy and stability can theoretically approach that of the Space Telescope.

2. Minimal Basebody and Payload/Payload Interactions -- the soft interface and lack of basebody reaction torques mitigate the issues of basebody flexible structure excitation and payload to payload interference. For simple (PD) payload controls, the system stability no longer depends on the basebody (provided the basebody is stable by itself) [39].

3. Supports Modular Design and Multi-Payload Accommodation -- since the basebody and payloads are mutually isolated from each other, the pointing needs of individual payloads can be met independent of the overall system configuration.

4. Potentially Low Cost -- expensive gimbals and magnetic or active flexure bearings are replaced by moderate cost reaction wheels or CMGs and a mechanically simple soft interface.

Analysis of potential designs [39,40] shows the feasibility of wideband disturbance rejection and sub-microradian pointing in a Space Station environment. A simple model of the power tower configuration was used, and allowed to oscillate in translation and rotation approximately 0.1 m and 0.1 degrees, respectively, using white noise band limited to 1 Hz. The payload was isolated by a 6 node PVF_2 system and had a 1 Hz bandwidth reaction wheel control system. Results indicated a payload stability of less than 0.05 microradians. Further details of the analysis of such systems to date may be found in [39,40].

5.0 CONCLUSIONS AND RECOMMENDATIONS

5.1 Summary

Large gimbal systems that have been flown, delivered and awaiting flight, or under fabrication are summarized in this subsection.

The Apollo Telescope Mount (ATM) was designed and developed for Skylab to house and support manned telescopes for studying the sun. It was a 10,000 kg octagonally shaped structure which surrounded a large cylindrical canister housing the scientific instruments of 1000 kg. The Skylab CMGs provided vehicle coarse pointing to within 3 arc-min and the center of mass mounted gimbal system of the ATM provided 3-axis fine pointing to 2.5 arc-seconds. The ATM was flown in 1973.

The Instrument Pointing System (IPS) is a gimbal system which is mounted on an open pallet sitting in the open bay of Shuttle. It provides 3 degrees of freedom to an end mounted payload of up to 2500 kg. When Shuttle is free from disturbances such as astronaut motions and thruster firing, IPS can achieve a pointing stability of about 4 arc-sec. However, its stability could degrade to 15 arc-seconds due to Shuttle vernier thruster firing alone. IPS was flown in 1985.

Cryogenic Infrared Radiance Instruments for Shuttle (CIRRIS-1) is a single axis pointing system for an infrared telescope system developed for the Air Force Geophysics Laboratory. It was designed to point a payload of about 600 kg with size of about 1 meter diameter by 3 meter length to an accuracy of 12 arc-minutes. With the Shuttle in a nose down attitude, CIRRIS-1 used the Shuttle orbital motion to provide a translational scan along the limb and a single axis pointing control to step through a sequence of tangent heights. Pointing stability achieved is 9 arc-sec.

CIRRIS-1A is a follow-on gimbal after CIRRIS-1 for the Air Force Geophysics Laboratory. But it is a two-axis azimuth-over-elevation gimbal used to carry instruments to measure IR radiance in the 2.5 to 25 micron region. CIRRIS-1A has a payload capacity of about 780 Kg with dimensions 1 meter diameter by 2.83 meters length to a pointing accuracy of 4 arc-min. Its pointing stability is expected to be less than 30 arc-sec. CIRRIS-1A was delivered for scheduled Shuttle flight STS-62A. Due to the Challenger accident, its flight has been delayed.

The Two Axis Pointing System (TAPS) is a C.M. mount two axis gimbal system currently under fabrication for NASA/Goddard Space Flight Center. TAPS is designed to provide 1 arc-min pointing accuracy for Shuttle payloads weighing up to 1135 kg and sizes up to 1 m by 1 m by 4.2 m length.

A pointer, in general, consists of sensors, actuators, control software, disturbance isolators, structural elements, and thermal controls. Technologies in these component areas relating to large pointing systems are summarized as follows:

Depending on field of view and star magnitude, a current star tracker is at arc-sec stability accuracy and its absolute accuracy varies depending on the tracker alignment relative to reference coordinates. However, Advanced Star and Target Reference Optical Sensor (ASTROS), a CCD-based star tracker, can achieve 0.1 arc-sec stability. For rotational rate and angle measurements, gyros of 0.2-0.01 arc-sec noise equivalent angle (NEA) are currently available. For example, NEA of the DRIRU II gyro is at 0.2 arc-sec and the Third Generation Gyro (TGG) of the Lincoln Experiment Satellite (LES 8 and 9) has an NEA of 0.01 arc-sec.

For actuations, torque level is an important parameter to consider, since it determines maximum acceleration and control bandwidth achievable. The CIRRIS-1A gimbal uses a flight ready D.C. brushless motor that can deliver an output torque of 130 newton-meters. The manufacturer of this motor has also produced D.C. brushless motors of 4000 newton-meters for ground use.

Primary control of spacecraft or pointing systems to date has all been based on classical control methodologies. Though modern state-space approaches have been used in flight, they are primarily limited to experiments.

Active isolators such as the Magnetic Bearing Assembly (MBA) and the Gimbal Flex are still being developed. However, small passive isolators such as the ones designed for isolating reaction wheel disturbances from Hubble Space Telescope (HST) are ready for flight.

In the recent Solar Optical Universal Polarimeter (SOUP) mission, Image Motion Compensation (IMC) was demonstrated to 0.003 arc-second stability on board the Shuttle. But there is no flight technology identified for thermal lines across gimbals. However, an engineering model of the Talon Gold gimbal did address the issue of a rotary fluid joint for active thermal cooling.

In addition to the conventional gimbaled option, pointers may be tethered from a Space Station. But tethered pointing is immature because there is no previous experience in this area. Tether Satellite System (TSS-1) is manifested for 1990, and a great deal can be learned from this first tether flight ever. But tethered pointing will not have a chance for flight test until the Kinetic Isolation Technology Experiment (KITE) is flown. Current plans call for a 1992 flight for KITE, but it is not manifested. Complex dynamics and safety issues must be completely understood before tether technology is declared mature.

5.2 Issues and Concerns

As gimbal yoke size increases and the Code E payload mass grows, the equivalent gimbal stiffness drops. Decreased gimbal stiffness will require use of controllers of decreased bandwidth, which will lead to decreased level of pointing performance. Current structure and mechanical bearing technologies limit the equivalent gimbal system stiffness to about 5 Hz, given the gimbal size of 2.5 meters by 3.0 meters and a payload of 3000 kg. This lowest vibration frequency of the gimbal system will set an undesired limit on pointer performance. An unconventional approach may be needed to meet Code E performance targets.

A number of significant dynamic disturbances of the Space Station must not interfere with pointing system mounted on station. A large base isolator between the pointer and the station can effectively separate the pointer from the disturbance environment. But currently no off-shelf large isolator exists to support large pointers.

Though the issue of thermal cooling through fluid rotary joint was addressed in the engineering model of Talon Gold, a great deal more must be learned in order to bring the technology to flight level.

Most pointer components have lifetimes of less than 7 years, even though some devices with no moving parts may achieve a lifetime of 12 years. Therefore, a pointer is not expected to achieve a lifetime of 20 years without change outs.

Currently pointing systems for space applications are built with no systematic modular design technology basis. In case of maintenance or failure, major sub-assembly or even the whole pointing system have to be changed out. This will have profound implications on orbit replacement requirements, system cost and operations.

In this study, Space Station environmental effects on pointer components or systems were not assessed. Since the pointer is not completely sealed and there are moving parts and optical sensors in the pointer, contamination effects on pointer performance and lifetime need to be assessed.

5.3 Conclusions

Systems such as CIRRIS-1, CIRRIS-1A, and TAPS do not meet all Code E requirements in performance, number of axes for pointing or payload size accommodation. IPS can accommodate large payloads, but would fail to meet stability requirements under disturbances. However, current systems do meet a subset of Code E requirements.

To design and build a large pointer to satisfy Code E requirements, technologies of certain components are available and flight ready. These are gyros, trackers, direct drive actuators, small passive isolators, control methodologies, image motion compensations, and small reaction wheels. But other component technologies are still at the brassboard level: they are reactionless actuators, low noise CMGs, vernier isolators, active base isolators, active thermal control across gimbal. Technologies that are not as far along as brassboard level are: large passive isolators, high stiffness mechanical bearings and high stiffness/weight ratio structural materials.

In summary, no gimbaled pointing system can be built today to meet Code E requirements from off-shelf components. Therefore, advanced development of technologies is required.

5.4 Recommendations

To accommodate Code E large payloads in a dynamically vibratory station environment and to meet the sub-arc-second pointing stability requirement, the following brassboard technology development should be accelerated: large passive isolators, vernier isolators, reactionless actuators, active thermal control, lightweight material for increased stiffness and damping, and bearing technology for large pointers.

DoD/SDIO has recently funded a number of programs for high performance pointing systems. For example, the Space Active Vibration Isolation (SAVI) program addresses most issues involving a precision pointer in a vibration environment. Technologies emerging from such DoD/SDIO pointing systems are applicable to pointers for Code E missions and therefore should be fully utilized.

The first tethered satellite system (TSS-1) is scheduled to fly on the Shuttle in 1990. A great deal can be learned from the TSS-1 flight, but no tethered pointing experiment (such as the Kinetic Isolation Tether Experiment, KITE), has been manifested. Therefore, tethered pointing technology will not be ready until after the mid 90s. For Code E payloads, tethered pointing may only be considered in late 1990s.

Since issues such as long lifetime of pointers, modular pointer designs, and station environmental effects are not addressed in this study, they should be investigated in the future.

REFERENCES:

1. R.A. Laskin, S.W. Sirlin, "Instrument Pointing Technology for Spaceborne Science Missions of the 1990s," IAA-84-2021, AIAA/AAS Astrodynamics Conference, August 20-22, 1984.

2. O.K. Garriott, D.L. Forsythe, E.H. Cagle, "Instruments, Systems and Manned Operations of the Apollo Telescope Mount," Astronautics & Aeronautics, June 1971, pp. 50-57.

3. Steven D. Fisher, Bruce Bollermann, "Cryogenic Infrared Radiance Instrumentation for Shuttle (CIRRIS) Pointing Control System," SPIE, Vol. 265, February 10-13, 1981, pp. 316-342.

4. D.R. Smith, A.T. Stair, Jr., A.J. Steed, D.A. Burt, "Cryogenic Infrared Radiance Instrumentation for Shuttle (CIRRIS)," SPIE, Vol. 265, February 10-13, 1981, pp. 310-315.

5. Capabilities in Flight Motion Simulation and Guidance and Navigational Test Equipment, Carco Electronics, 195 Constitution Drive, Menlo Park, California, 94025.

6. Pointing And Isolation Systems Brochure, Sperry Corporation Aerospace and Marine Group, P.O. Box 21111, Phoenix, Arizona, 85036, pub. no. 41-7200-00-86, September 1985.

7. Douglas Havernhill, Kevin D. Kral, "Payload Isolation Using Magnetic Suspension," American Astronautical Society Guidance And Control Conference, AAS 85-104, February 2-6, 1985.

8. Norman A. Osborne, "Gimbalflex 5-Degree of Freedom Inertially Stabilized Platform", American Astronautical Society Guidance And Control Conference, AAS 80-024, February 1980.

9. L.P. Davis, J.F. Wilson, R.E. Jewell, J.J. Roden, "Hubble Space Telescope Reaction Wheel Assembly Vibration Isolation System," Sperry Corporation Aerospace and Marine Group, P.O. Box 21111, Phoenix, Arizona, 85036.

10. S.R. Sadin, NASA Space Systems Technology Model, NASA TM 88176, Volume 2-Data Base Technology Analysis, Sixth Edition, June 1985.

11. Military Space Systems Technology Model (U), (unclassified portion of a larger document), SD-TR-82-01-VOL-3A, 1983.

12. S.W. Sirlin, and R.A. Laskin, "Payload Isolation and Pointing for the 1990s," Proceedings of the Rocky Mountain Guidance and Control Conference, Keystone, Colorado, February 1985.

13. R.A. Laskin, S.W. Sirlin, "Future Payload Isolation and Pointing and System Technology," J. Guidance, Vol. 9, No. 4, July-August 1986, pp. 469-477.

14. W. C. Goss, "Fiber Optic Gyro Development at the Jet Propulsion Laboratory," SPIE, Vol. 719, Fiber Optic Gyros: 10th Anniversary Conference, 1986, pp. 113-121.

15. R.L. De Paula, JPL Presentation Material (JPL Internal Document), Jet Propulsion Laboratory, Pasadena, California, 1987.

16. R.H. Stanton, J.W. Alexander, E.W. Dennison, T.A. Glavich, P.M. Salomon, R.E. Williamson, "ASTROS: A Sub-arc-sec CCD Star Tracker," SPIE Proceedings, Vol. 50, August 1984.

17. R.A Laskin, E.H. Kopf, S.W. Sirlin, J.T. Spanos, P.J. Wiktor, "Reactionless Gimbal Actuation for Precision Pointing of Large Payloads," AAS/AIAA Astrodynamics Specialist Conference, AAS 87-512, August 10-13, 1987.

18. R. Van Riper, "Future Technology Trends for Control Moment Gyroscopes," AIAA Guidance, Navigation and Control Conference, 2207-CP, August 18-20, Williamsburg, Virginia.

19. J.R. Kendig, P. Davis, "Space-Qualified 1000 Foot-Pound-Second Magnetically Suspended Reaction Wheel Assembly (MSRWA)," American Astronautical Society Guidance and Control Conference, AAS-81-023, January 1-February 4, 1981.

20. Momentum and Control Systems Brochures, Sperry, pub. no. PT7200-84, and Control Moment Gyros, Sperry, pub. no. 61-1720-08-00.

21. A. Scott Hamilton, Bendix Presentation Material, Guidance Systems Division, undated.

22. Inland Motor Catalogue, Specialty Division of Koll Morgen Corp., 501 First Street, Radford, Virginia 24141, 1982.

23. Brian J. Hogan, "Reactionless Beamsteering Mirror May Aim Lasers for SDI," Design News, September 8, 1986, pp. 104-108.

24. Banavar Sridhar, Jean-Noel Aubrun, Kenneth R. Lorell, "Design of a Precision Pointing Control System for the Space Infrared Telescope Facility," IEEE Control Systems Magazine, February 1986.

25. T.D. Tarbell, D.W. Duncan, M.L. Finch, "Image Motion Compensation on the Spacelab 2 Solar Optical Universal Polarimeter (SL2 SOUP)," SPIE, Vol. 265, Supplement-Shuttle Pointing of Electro-Optical Experiments, 1981, pp. 39-46.

26. Damping 1986 Proceedings, AFWL-TR-86-3059, 2 Volumes.

27. S.P. Rawal and M.S. Misra, "Material Damping in Space Structures," Damping 1986 Proceedings, Vol. 2, pp. FB1-9.

28. S.P. Rawal, M.S. Misra, Final Report: Interfaces and Damping in Metal Matrix Composites, Martin Marietta, MCR-86-684.

29. Applications of Tethers in Space, Workshop Proceedings, NASA Conference Publication 2422, 2 Volumes, 1985.

30. E. Turci, "Tether Pointing Platform and Space Elevator Mechanisms Analysis of the Key Concepts for SATP and Scaled SATP," ibid. Vol. 2, pp. 287-324.

31. "Tethered Elevator and Platforms as Space Station Facilities: System Studies and Demonstrative Experiments," (Panel Presentation), ibid. Vol. 2, pp. 413-455.

32. L. Lemke, "Tether System Study Report," presented at OSSA Space Station Pointing Study Working Group, July 16, 1988.

33. E. Fukada, S. Takashita, "Piezoelectric Effect in Poly (vinylidene fluoride), Japan J. Appl. Phys., Vol. 8, No. 7, 1969, p. 960.

34. H. Kawai, "The Piezoelectricity of Poly (vinylidene fluoride)", Japan J. Applied Physics, Vol. 8, 1969, p. 975.

35. M.A. Marcus, "Ferroelectric Polymers and their Applications," presented at Fifth International Meeting on Ferroelectricity at Pennsylvania State University, August, 1981.

36. T. Bailey, J.E. Hubbard, Jr., "Distributed Piezolectric Polymer Active Vibration Control of a Cantilever Beam," AIAA Journal of Guidance, Control, and Dynamics, Vol. 8, No. 5, 1985, pp. 605-611.

37. Kynar Piezo Film Technical Manual, Pennwalt Corporation, includes many further references, 1987.

38. J.A. Simpson, and A.J. Tuzzolino, "Polarized Polymer Films as Electronic Pulse Detectors of Cosmic Dust Particles," Journal of Nuclear Instruments and Methods, Vol. 236, No. 1, May 1985, pp. 187-202.

39. S.W. Sirlin, R.A. Laskin, "The Softmounted Inertially Reacting Pointing System (SIRPNT)," presented at AAS Guidance and Control Conference, Keystone, Colorado, February 1986.

40. S.W. Sirlin, "Piezoelectric Polymer-Based Isolation Mount for Articulated Pointing Systems on Large Flexible Spacecraft," presented at AAS/AIAA Astrodynamics Specialist Conference, Kalispell, Montana, August 1987.

NASA
FORMAL
REPORT

FFNo 665 Aug 65